# AUTHOR QUERY FORM

**Journal:** CELL

**Article Number:** 8163

Dear Author,

Please check your proof carefully and mark all corrections at the appropriate place in the proof.

| Location in article | Query / Remark: Click on the Q link to find the query's location in text<br>Please insert your reply or correction at the corresponding line in the proof |
|---|---|
| | There are no queries in this article |

Thank you for your assistance.

Article

Cell

# Acyl-CoA Dehydrogenase Drives Heat Adaptation by Sequestering Fatty Acids

## Graphical Abstract

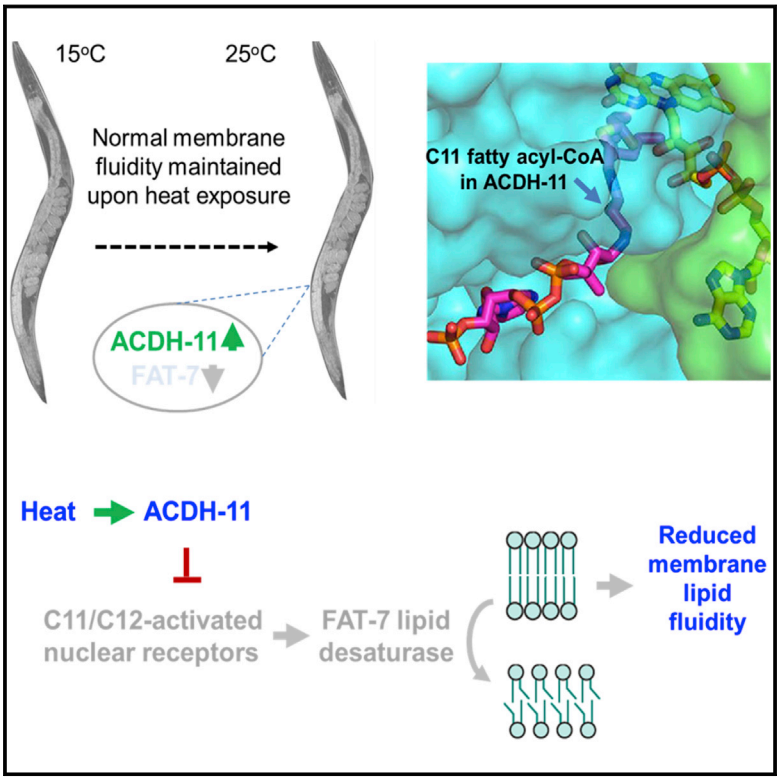


## Authors

Dengke K. Ma, Zhijie Li, ..., Fei Sun, H. Robert Horvitz

## Correspondence

dengke.ma@ucsf.edu (D.K.M.), horvitz@mit.edu (H.R.H.)

## In Brief

Cells must adjust lipid saturation levels to maintain membrane fluidity upon temperature change. A highly conserved lipid metabolism protein links these processes in *C. elegans* by sequestering fatty acids from the transcriptional activator of a lipid desaturase when temperatures rise.

## Highlights

- ACDH-11 upregulation sequesters C11/12 fatty acids to drive heat adaptation
- Decreased C11/12 fatty acids downregulate FAT-7 fatty acid desaturase
- Reduced levels of membrane desaturated fatty acids reduce membrane fluidity
- The *acdh-11* phenotype models a thermo-sensitive syndrome caused by ACDH deficiency

Ma et al., 2015, Cell *161*, 1–12
May 21, 2015 
http://dx.doi.org/10.1016/j.cell.2015.04.026

CellPress

Please cite this article in press as: Ma et al., Acyl-CoA Dehydrogenase Drives Heat Adaptation by Sequestering Fatty Acids, Cell (2015), http://dx.doi.org/10.1016/j.cell.2015.04.026



Cell

# Acyl-CoA Dehydrogenase Drives Heat Adaptation by Sequestering Fatty Acids

Dengke K. Ma,[1,6,*] Zhijie Li,[2] Alice Y. Lu,[1] Fang Sun,[2] Sidi Chen,[3] Michael Rothe,[4] Ralph Menzel,[5] Fei Sun,[2] and H. Robert Horvitz[1,3,*]

[1]Department of Biology, Howard Hughes Medical Institute, McGovern Institute for Brain Research, Massachusetts Institute of Technology, Cambridge, MA 02139, USA

[2]National Laboratory of Biomacromolecules, Institute of Biophysics, Chinese Academy of Sciences, Beijing 100101, China

[3]Koch Institute for Integrative Cancer Research, Massachusetts Institute of Technology, Cambridge, MA 02139, USA

[4]Lipidomix GmbH, Robert-Roessle-Strasse 10, 13125 Berlin, Germany

[5]Department of Biology, Freshwater and Stress Ecology, Humboldt-Universität zu Berlin, Spaethstrasse 80/81, 12437 Berlin, Germany

[6]Present address: Department of Physiology, Cardiovascular Research Institute, UCSF School of Medicine, San Francisco, CA 94158-9001, USA

*Correspondence: dengke.ma@ucsf.edu (D.K.M.), horvitz@mit.edu (H.R.H.)

http://dx.doi.org/10.1016/j.cell.2015.04.026

## SUMMARY

Cells adapt to temperature shifts by adjusting levels of lipid desaturation and membrane fluidity. This fundamental process occurs in nearly all forms of life, but its mechanism in eukaryotes is unknown. We discovered that the evolutionarily conserved *Caenorhabditis elegans* gene *acdh-11* (acyl-CoA dehydrogenase [ACDH]) facilitates heat adaptation by regulating the lipid desaturase FAT-7. Human ACDH deficiency causes the most common inherited disorders of fatty acid oxidation, with syndromes that are exacerbated by hyperthermia. Heat upregulates *acdh-11* expression to decrease *fat-7* expression. We solved the high-resolution crystal structure of ACDH-11 and established the molecular basis of its selective and high-affinity binding to C11/C12-chain fatty acids. ACDH-11 sequesters C11/C12-chain fatty acids and prevents these fatty acids from activating nuclear hormone receptors and driving *fat-7* expression. Thus, the ACDH-11 pathway drives heat adaptation by linking temperature shifts to regulation of lipid desaturase levels and membrane fluidity via an unprecedented mode of fatty acid signaling.

## INTRODUCTION

How cells respond to changes in temperature is a fundamental issue in biology (de Mendoza, 2014; Jordt et al., 2003; Sengupta and Garrity, 2013). Changes in ambient temperature affect nearly all cellular and biochemical processes and drive adaptive responses to maintain cellular homeostasis. For example, up- or down-shifts in temperature increase or decrease the fluidity of the cytoplasmic membrane, respectively. To maintain membrane fluidity within an optimal range for normal biological activity, lipid desaturases in the cell convert saturated fatty acids into unsaturated fatty acids to increase lipid desaturation and thus membrane fluidity in response to temperature downshifts (de Mendoza, 2014; Flowers and Ntambi, 2008; Holthuis and Menon, 2014; Nakamura and Nara, 2004; Zhang and Rock, 2008). Unsaturated double bonds in lipids generate kinks into the otherwise straightened acyl hydrocarbon chain and thereby increase membrane fluidity. This fundamental process of maintaining membrane fluidity is called homeoviscous adaptation (HVA) and occurs in bacteria, archaea, and eukaryotes (Anderson et al., 1981; Cossins and Prosser, 1978; Shmeeda et al., 2002; Sinensky, 1974).

A two-component regulatory system mediates HVA in bacteria (Aguilar et al., 2001; de Mendoza, 2014; Holthuis and Menon, 2014; Zhang and Rock, 2008). In *Bacillus subtilis*, temperature down-shifts induce the expression of the *des* gene, which encodes a lipid desaturase, Des. This induction is controlled by the DesK-DesR two-component system: upon temperature down-shift, the transmembrane histidine kinase DesK phosphorylates and activates the response regulator DesR, which stimulates transcription of *des*. Activation of the DesK-DesR pathway enhances the survival of *Bacillus subtilis* at low temperatures. Whether regulation of lipid desaturation by this pathway is involved in heat adaptation remains unclear. Furthermore, neither DesK nor DesR has apparent homologs in eukaryotes, and specific biological pathways leading to lipid desaturase regulation and HVA in eukaryotes remain unknown.

The nematode *Caenorhabditis elegans* is an ectotherm, i.e., its body temperature depends on external sources. *C. elegans* survives and reproduces optimally over an environmental temperature range of 15°C and 25°C. Temperatures beyond this range cause physiological stress, reduction of fecundity, tissue damage, and necrosis (Kourtis et al., 2012; van Oosten-Hawle and Morimoto, 2014). Previous studies of *C. elegans* thermoregulation have focused on understanding how the heat-shock transcription factor HSF-1 functions to maintain proteostasis and cytoskeletal integrity (Baird et al., 2014; van Oosten-Hawle and Morimoto, 2014; van Oosten-Hawle et al., 2013) and on sensory neural circuits and thermotaxis behavioral strategies that allow the animal to navigate a temperature gradient (Garrity et al., 2010; Hedgecock and Russell, 1975; Mori and Ohshima, 1995;

Sengupta and Garrity, 2013). Although the *C. elegans* genome encodes seven lipid desaturases that are evolutionarily conserved and involved in fatty acid regulation (Brock et al., 2006; Watts, 2009), the functions and mechanisms of HVA in *C. elegans* have not been explored.

We identified the *C. elegans* gene *acdh-11* (acyl-CoA dehydrogenase) from a genetic screen exploring how this animal responds to conditions of changing oxygen and subsequently discovered that *acdh-11* functions in HVA and does so by regulating levels of the stearic Co-A desaturase (SCD) FAT-7. *acdh-11* encodes a member of the evolutionarily conserved ACDH family, which is broadly involved in lipid β-oxidation. To understand the mechanism of action of ACDH-11, we solved its high-resolution crystal structure. This structure helped us establish that ACDH-11 inhibits *fat-7* expression by sequestering C11/C12-chain fatty acids and preventing them from activating *fat-7* expression mediated by the nuclear hormone receptor (NHR) NHR-49, a *C. elegans* homolog of the mammalian fatty acid-binding transcription factors HNF4α and PPARα (Antebi, 2006; Ashrafi, 2007; Atherton et al., 2008; Evans and Mangelsdorf, 2014; Van Gilst et al., 2005). Our findings demonstrate that specific intracellular fatty acids link ACDH-11 in a metabolic pathway to NHRs for transcriptional control of homeoviscous heat adaptation in *C. elegans.* We propose that these molecular principles and mechanisms are evolutionarily conserved and modulate membrane lipid homeostasis and heat adaptation in other organisms.

## RESULTS

### *acdh-11* Is Required for Heat Adaptation

We previously reported that the *C. elegans* gene *egl-9* controls a behavioral response to reoxygenation (the O2-ON response) by regulating fatty acid-eicosanoid signaling (Ma et al., 2012, 2013). We examined other *egl* mutants originally isolated based on egg-laying behavioral defects (Trent et al., 1983) and discovered that the previously uncloned gene *egl-25* is also required for both normal egg laying and the O2-ON response (Figures S1A–S1E). We molecularly identified *egl-25* (Figures 1A and S1A–S1E) as the gene *paqr-2* (progestin and adipoQ receptor-2), the sequence of which has similarity to those of mammalian adiponectin receptors and which promotes the adaptation of *C. elegans* to cold temperature (Svensk et al., 2013; Svensson et al., 2011). Since the molecular function of this gene is unclear, we continue to refer to it by its original name, *egl-25*. We confirmed that *egl-25* promotes cold adaptation and the intestinal expression of the SCD gene *fat-7* (Svensk et al., 2013; Svensson et al., 2011) (Figures S1C and S1F).

We expressed a $P_{fat\text{-}7}$*::fat-7::GFP* fluorescent reporter (*nIs590*) in the *egl-25* mutant background to seek *egl-25* suppressor mutations that can restore *fat-7* levels (see Experimental Procedures). We isolated over 40 mutations that suppress *egl-25*, eight of which (*n5655*, *n5657*, *n5661*, *n5876*, *n5877*, *n5878*, *n5879*, *n5880*) belong to one complementation group and are alleles of a functionally uncharacterized gene named *acdh-11* (Figure 1A). The amino acid sequence of ACDH-11 suggests that it is a long-chain ACDH involved in fatty acid β-oxidation (Ashrafi, 2007; Srinivasan, 2015). *acdh-11* genetically interacts with *acs-3*, which encodes an acyl-CoA synthetase (Ashrafi, 2007; Mullaney et al., 2010). The eight mutations we isolated include one deletion allele and three missense mutations, each of which disrupts an amino acid residue completely conserved among ACDH protein family members (Figures 1B and S2). Such loss-of-function mutations of *acdh-11* restored only slightly the behavioral defects (in egg laying and the O2-ON response) of *egl-25* mutants but caused dramatic upregulation of $P_{fat\text{-}7}$*::fat-7::GFP* in both *egl-25* mutant and wild-type backgrounds (Figures 1C and 1D).

Because *fat-7* encodes an SCD that catalyzes the limiting step of lipid desaturation and promotes membrane fluidity (de Mendoza, 2014; Flowers and Ntambi, 2008), we monitored the extent of membrane fluidity in *acdh-11* mutants using the fluorescent dye di-4-ANEPPDHQ (Owen et al., 2012). We found that the fluorescence spectrum of di-4-ANEPPDHQ was red-shifted (Figure S3A), suggesting increased membrane fluidity. Using liquid chromatography-mass spectroscopy (LC-MS) to quantify endogenous levels of various fatty acids, we found that *acdh-11* mutants were abnormal in their compositions of specific fatty acid species (Figure 2A). In particular, we observed a markedly reduced level of stearic acid (C18:0, 18 carbon atoms and 0 double bonds), which is the most abundant saturated fatty acid in *C. elegans* (Figure 2A). The reduced level of C18:0, the metabolic substrate of FAT-7, is consistent with overexpression of $P_{fat\text{-}7}$*::fat-7::GFP* in *acdh-11* mutants. These data indicate that ACDH-11 functions to decrease *fat-7* expression, the desaturation of the FAT-7 substrate stearic acid and membrane lipid fluidity.

Because changes in membrane fluidity are essential for adaptation to temperature shifts, we next examined the temperature sensitivity of *acdh-11* mutants. We found that *acdh-11* mutant embryos successfully developed to adulthood at 15°C or 20°C but failed to do so at 25°C (Figures 2B and 2C). Transgenic expression of wild-type *acdh-11(+)* or decreasing membrane fluidity by supplementing *acdh-11* mutants with the membrane-rigidifying agent DMSO (Lyman et al., 1976; Sangwan et al., 2001) or reducing the *fat-7* expression level by mutation rescued the 25°C growth defect (Figure 2C). Since temperature higher than 25°C causes heat stress, tissue necrosis and damage in *C. elegans* (Kourtis et al., 2012; van Oosten-Hawle and Morimoto, 2014), we also examined survival of *C. elegans* adults at 37°C and found that *acdh-11* mutants but not *acdh-11*; *fat-7* double mutants exhibited increased death rates compared with wild-type animals (Figure 2D). By contrast, both *acdh-11* mutants and the wild-type exhibited similar sensitivity to other types of stress, including high osmolality and oxidative stress (Figures S3B and S3C). These results indicate that ACDH-11 promotes *C. elegans* heat adaptation (also see below) by regulating *fat-7* expression and membrane fluidity.

### High Temperature Upregulates *acdh-11* Expression to Decrease *fat-7* Expression

We generated a transcriptional reporter strain ($P_{acdh\text{-}11}$*::GFP*) with *GFP* driven by the 0.6 kb promoter of *acdh-11*. We observed that growth at 25°C as opposed to 20°C or 15°C caused marked upregulation of $P_{acdh\text{-}11}$*::GFP* predominantly in the intestine (Figure 3A), the site of *fat-7* expression, suggesting that ACDH-11

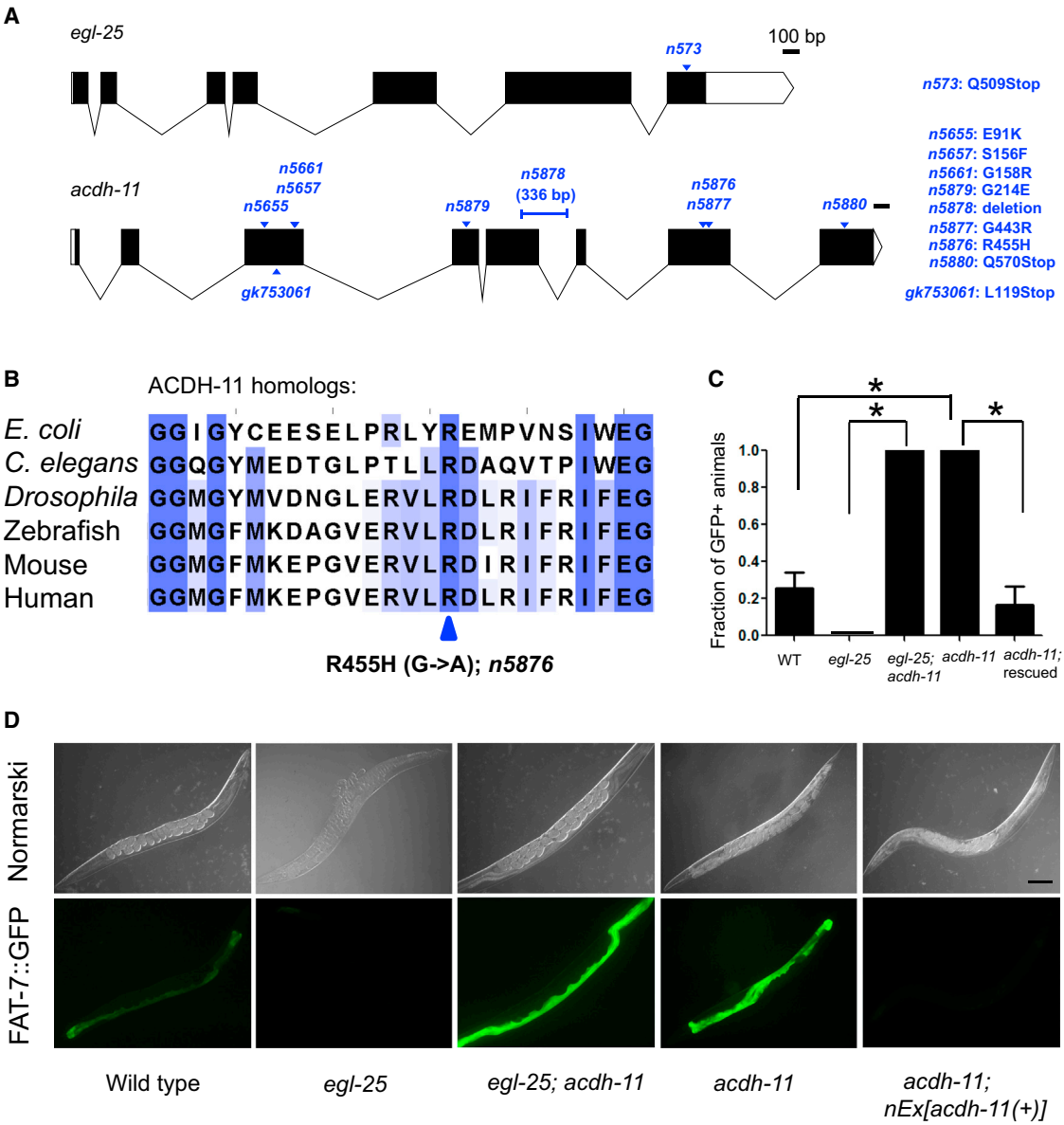


**Figure 1. *acdh-11* Regulates *fat-7* Expression**

(A) Schematic of *egl-25* and *acdh-11* gene structures. Shown are *egl-25(n573)*, *acdh-11(gk753061)*, and another eight *acdh-11* mutations isolated from *egl-25(n573)* suppressor screens. Both *n573* and *n5880* are ochre (CAA-to-TAA) mutations and *gk753061* is an amber (TTG-to-TAG) mutation.

(B) Sequence alignments of ACDH-11 homologs from *Escherichia coli* (AidB), *Drosophila melanogaster* (CG7461), *Danio rerio* (Acadvl), *Mus musculus* (Acadvl), and *Homo sapiens* (ACADVL). For clarity, only the regions corresponding to that surrounding amino acid residue R455, which is disrupted by the *acdh*-11 mutation *n5876,* are shown. The three shades of blue indicate the degree of amino acid identity (deep blue >80%; blue >60%; light blue >40%). Arrow indicates the completely conserved R455 residue, which is disrupted by the *acdh-11(n5876)* mutation.

(C) Fractions of animals expressing FAT-7::GFP at 20°C as scored visually. $p < 0.01$ (n = 100 for each of five independent experiments).

(D) EGL-25 and ACDH-11 antagonistically regulate the abundance of the *nIs590[$P_{fat-7}$::fat-7::GFP]* reporter (FAT-7::GFP). Representative Nomarski and GFP fluorescence micrographs are shown of *C. elegans* adults of the genotypes indicated and grown at 20°C. Alleles used were: *egl-25(n573)*, *egl-25(n573); acdh-11(n5655)*, and *acdh-11(n5878)*.

See also Figures S1 and S2.

regulates *fat-7* cell-autonomously. Quantitative PCR (qPCR) revealed an ~2-fold induction of endogenous *acdh-11* transcripts at 25°C compared with 15°C (Figure 3B). By contrast, *fat-7* expression in the wild-type was strongly decreased at 25°C but increased in *acdh-11* mutants, based upon both RNA sequencing (RNA-seq) and qPCR experiments (Figures 3C and 3D). This regulation of *fat-7* by *acdh-11* is highly specific to *acdh-11*, since knockdown of *acdh-11* but not of the other 12

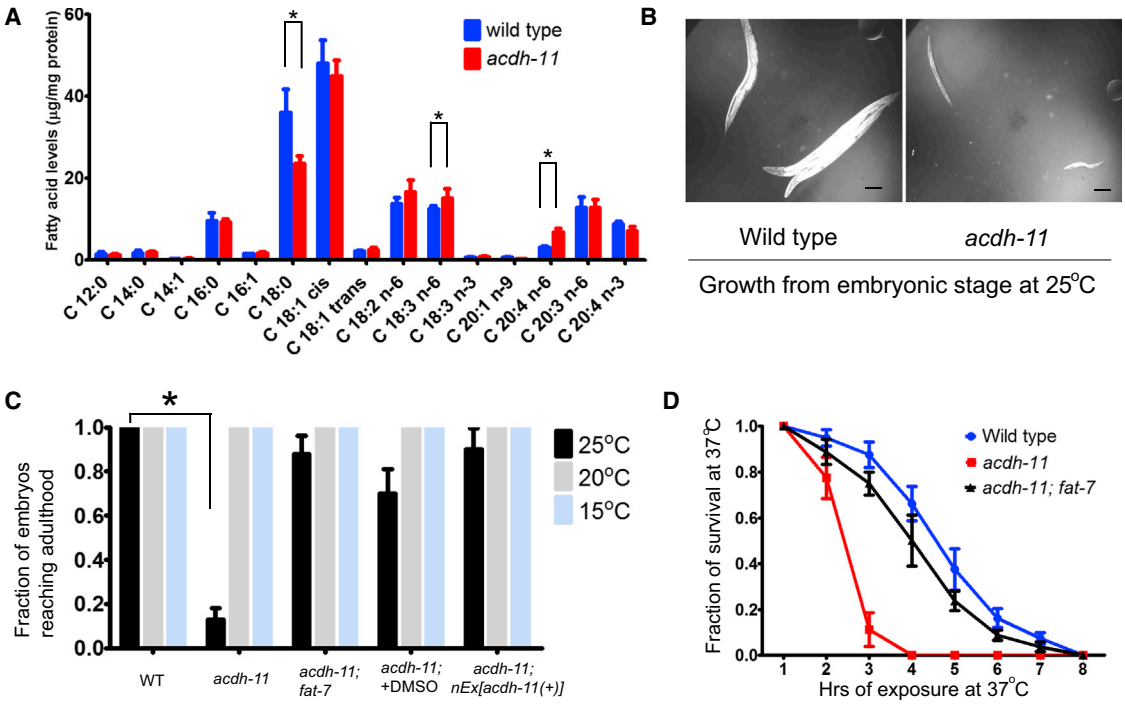


**Figure 2. ACDH-11 Regulates Lipid Desaturation and Promotes *C. elegans* Survival at High Temperature**

(A) LC-MS profiling of fatty acids extracted from young adult *C. elegans* populations of the wild-type and *acdh-11(gk753061)* null mutants. Fatty acids are indicated in the form C:D, where C is the number of carbon atoms in the fatty acid and D is the number of double bonds in the fatty acid. Fatty acid levels were normalized to total protein levels in the wild-type and *acdh-11* mutants ($p < 0.01$ from four independent samples for each genotype).

(B) Bright-field images showing the arrest of larval development of *acdh-11(gk753061)* null mutants but not of wild-type animals grown at 25°C. Bleach-synchronized embryos were grown for 4 days at 25°C.

(C) Fractions of embryos of indicated genotypes or treatment that developed to adulthood at 25°C (under the same conditions as in (B). $p < 0.01$ ($n = 20$ for each of four independent experiments).

(D) Fractions of adults that survived 37°C heat stress after shifting animals (24 hr post-L4) from 15°C to 37°C. After 24 hr recovery at 15°C, animals without pumping and responses to repeated touch were considered dead and counted for quantification. Error bars, SDs ($n = 50$ for each of four independent experiments). Statistical details in Supplemental Information. Scale bars, 100 µm.

See also Figure S3.

members of the *acdh* gene family in *C. elegans* by RNAi caused *fat-7* upregulation (Figures 3E and 3F). Temperature and *acdh-11* affected *fat-7* expression far more than expression of other *C. elegans fat* genes encoding lipid desaturases, including *fat-5* and *fat-6*, two close *fat-7* homologs in *C. elegans* (Figure 3C) (Murray et al., 2007; Watts, 2009). These results demonstrate upregulation of *acdh-11* by heat and a highly gene-specific function for *acdh-11* and elevated temperature in regulating the expression of *fat-7*, a member of the lipid desaturase gene family. These findings are consistent with the hypothesis that *acdh-11* and *fat-7* act in a pathway to facilitate *C. elegans* heat adaptation.

## ACDH-11 Crystal Structure Reveals the Basis of ACDH-11 Interaction with C11/C12-Chain Fatty Acids

To understand the mechanism of action of ACDH-11, we solved its 3D crystal structure as well as its structure in a complex with acyl-CoA (Figure 4; Table S1). Recombinant *C. elegans* ACDH-11 was expressed from *Escherichia coli*, purified and crystallized (Li et al., 2010). The structure of ACDH-11 was determined by molecular replacement, and the final atomic model of ACDH-11 was refined to 2.27 Å and 1.8 Å resolutions for the apo and the complex structures, respectively (Table S1). The overall structure is tetrameric (Figure 4A), consistent with our previous observation that the purified recombinant ACDH-11 (70 kDa monomer) is a 264 kDa protein in solution (Li et al., 2010). The monomer has an overall fold similar to that of its two described homologs, the *E. coli* alkylation response protein AidB (Bowles et al., 2008) and the human very long chain acyl-CoA dehydrogenase (VLCAD) (McAndrew et al., 2008). Each ACDH-11 monomer consists of an N-terminal α-helical domain (residues 1–200, α-domain 1), a seven-stranded β sheet domain (residues 201–320, α-domain 2), a central α-helical domain (residues 321–480, α-domain 3), and a C-terminal α-helical domain (Figure 4B). The tetramer comprises a dimer of dimers, with each subunit providing two loops important for stabilizing the dimer-dimer interaction (Figures 4A and S4A–S4E).

Long-chain ACDHs catalyze the initial step of fatty acid β-oxidation, the dehydrogenation of acyl-CoAs, with substrate-binding pockets that accommodate long-chain fatty acids of

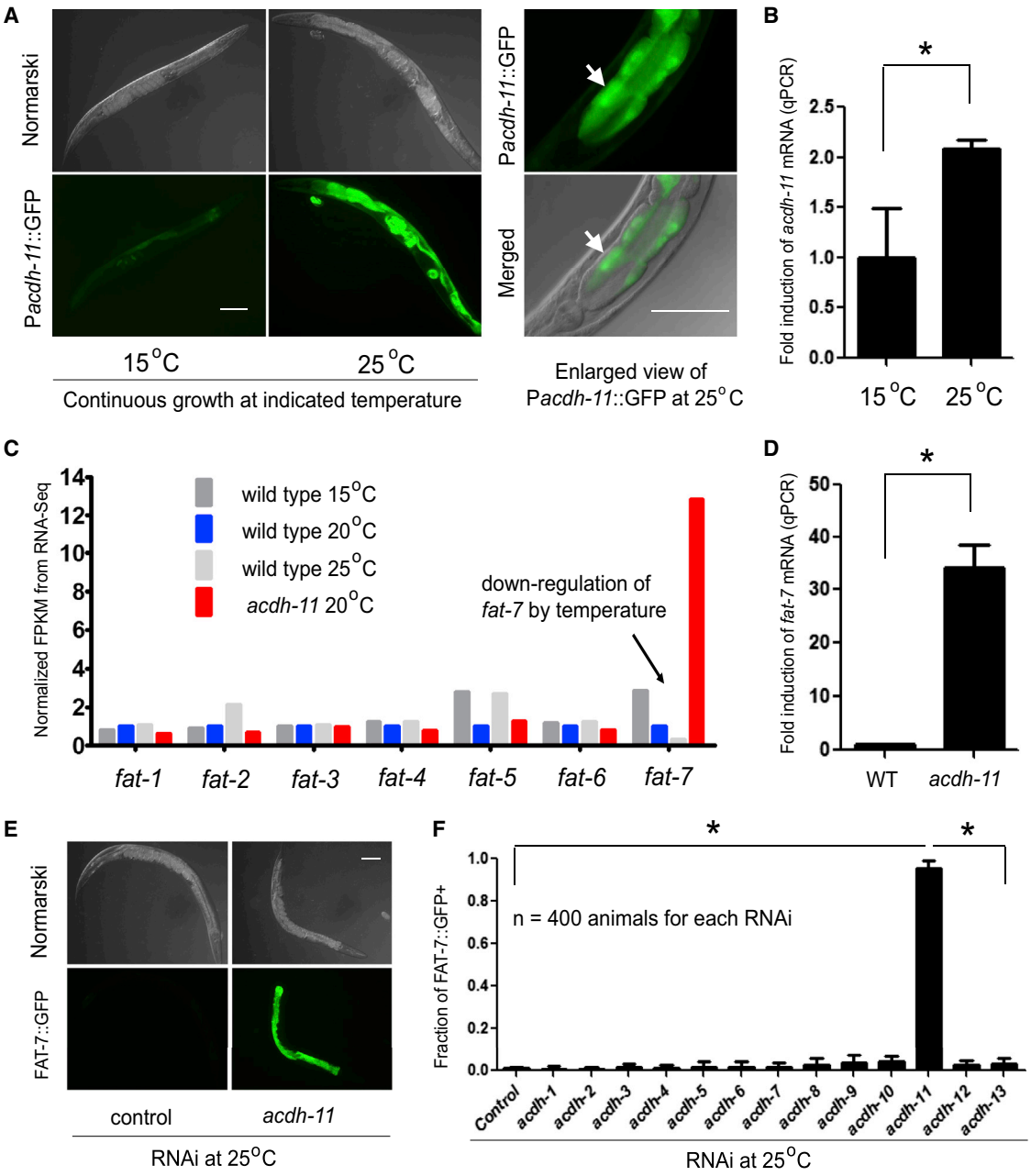


**Figure 3. Temperature Upregulates *acdh-11*, Causing Downregulation of *fat-7* Expression**

(A) Representative Nomarski and GFP fluorescence micrographs of wild-type transgenic animals with *nIs677[$P_{acdh-11}$::GFP]* (left), the expression of which is upregulated by high temperature at 25°C. A high-magnification view of another animal (right) shows GFP predominantly in intestinal cells (arrows). Scale bars, 100 μm.

(B) qPCR results showing that endogenous *acdh-11* is transcriptionally upregulated at 25°C. $p < 0.01$ (n = 4 for each genotype).

(C) RNA-Seq quantification of the expression levels at 15°C, 20°C, and 25°C (normalized to levels at 20°C) of genes encoding all seven *C. elegans* lipid desaturases (*fat-1* to *fat-7*). Arrow indicates downregulation of *fat-7* expression by temperature. FPKM, fragments per kilobase of exon per million fragments mapped.

(D) qPCR quantification showing *fat-7* expression levels in wild-type animals and *acdh-11* mutants. $p < 0.01$ (n = 4 for each genotype).

(E) Representative Nomarski and GFP fluorescence micrographs of wild-type *nIs590* transgenic animals showing that RNAi against *acdh-11* induces FAT-7::GFP expression at 25°C. Scale bars, 100 μm.

(F) RNAi against all *acdh* gene family members showing that *acdh-11* was specifically required for downregulating FAT-7 abundance at 25°C. $p < 0.01$ (n = 100 for each of four independent experiments).

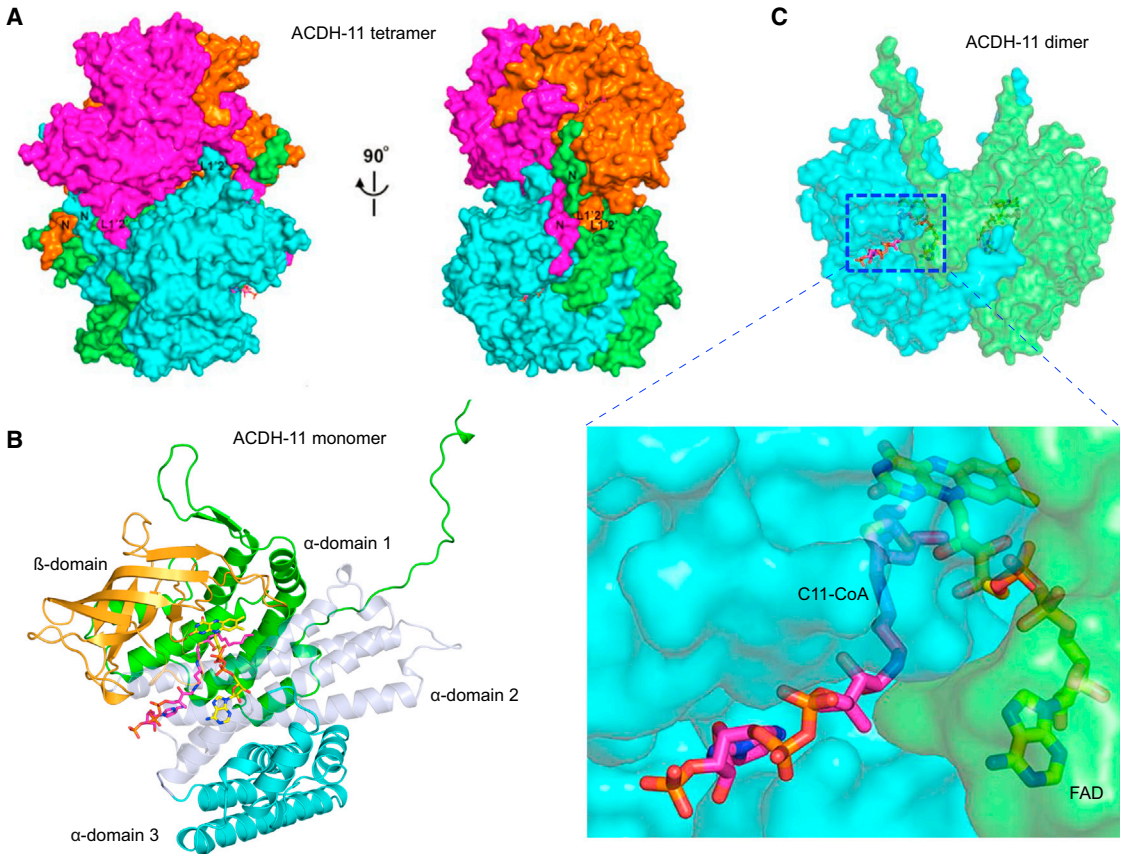


**Figure 4. Structure of ACDH-11 Showing Its Binding to the Fatty Acid C11-CoA**

(A) Surface representation of ACDH-11 tetramers showing a dimer of dimers: green-cyan and magenta-orange. For each subunit, the N-terminal loop and the L1′2′ loop are shown to form the dimer-dimer interface.

(B) Ribbon representation of an ACDH-11 monomer showing four domains (α-domain 1, 2, 3, and β-domain).

(C) Surface representation of an ACDH-11 dimer with an enlarged view of the ligand-binding cavity bound to C11-CoA. FAD, the enzymatic co-factor present in the crystal, is also shown and labeled.

See also Figure S4 and Table S1.

varying alkyl chain lengths (Grevengoed et al., 2014). To determine how the interaction of ACDH-11 with its substrates likely impacts HVA, we analyzed the classes of fatty acids that bind to the lipid binding pocket of ACDH-11. We found that ACDH-11 harbored the acyl chain of the fatty acid C11-CoA as a ligand in the crystal (Figures 4C and 5A–5E). C11-CoA was deeply buried inside a 14 Å-depth binding cavity of ACDH-11, the depth of which was restricted by two residues, Tyr344 and Leu159, limiting the maximum carbon length to C12 (Figures 4C and 5A). The temperature B-factors (Woldeyes et al., 2014), which indicate the motilities of these two amino acids (Tyr 344 and Leu 159), are relatively low across the entire ACDH-11 sequence (Figure 5B). The ligand-free apo-structure of ACDH-11 displays the same conformation of Tyr 344 and Leu 159 (Figures S5C and S5D), further supporting the conclusion that the size of the binding cavity would not accommodate fatty acid carbon lengths longer than C12.

The structure reveals that strong binding of ACDH-11 to C11-CoA is mediated by at least ten hydrogen bond interactions (Figure 5A), including one between Ser 267 and the 3′-phosphate on the CoA moiety; two between the side chain of Asn 331 and the N2 and N3 nitrogens of the adenine ring; two between the side chain of Arg 321 and the O4 and O5 oxygens in the adenosine 3′,5′-diphosphate group; two between the side chain of Arg 476 and the O9 and O10 oxygens of the pyrophosphate portion; two between the side chain of Arg334 and the O1 and O2 oxygens of the peptidyl portion; and one between the main chain of Ser215 and the N2 nitrogen of the peptidyl portion. We compared the structure of ACDH11 bound with C11-CoA with other structurally characterized ACDHs (SCAD, MCAD, and VLCAD) (Battaile et al., 2002; Kim et al., 1993; McAndrew et al., 2008) and found that ACDH-11 provides more hydrogen bonds (Figure S6) than other ACDHs and binds to the acyl chain via hydrophobic interactions that are defined by a deep binding pocket (Figure 5A). Using isothermal titration calorimetry (ITC), we quantified the binding affinities of C12-CoA and C8, C10, C12 fatty acids (we tested these even number chain-fatty acids, since their synthetic forms are readily available) to purified ACDH-11. The ITC results (Figures 5C–5E) showed that the disassociation

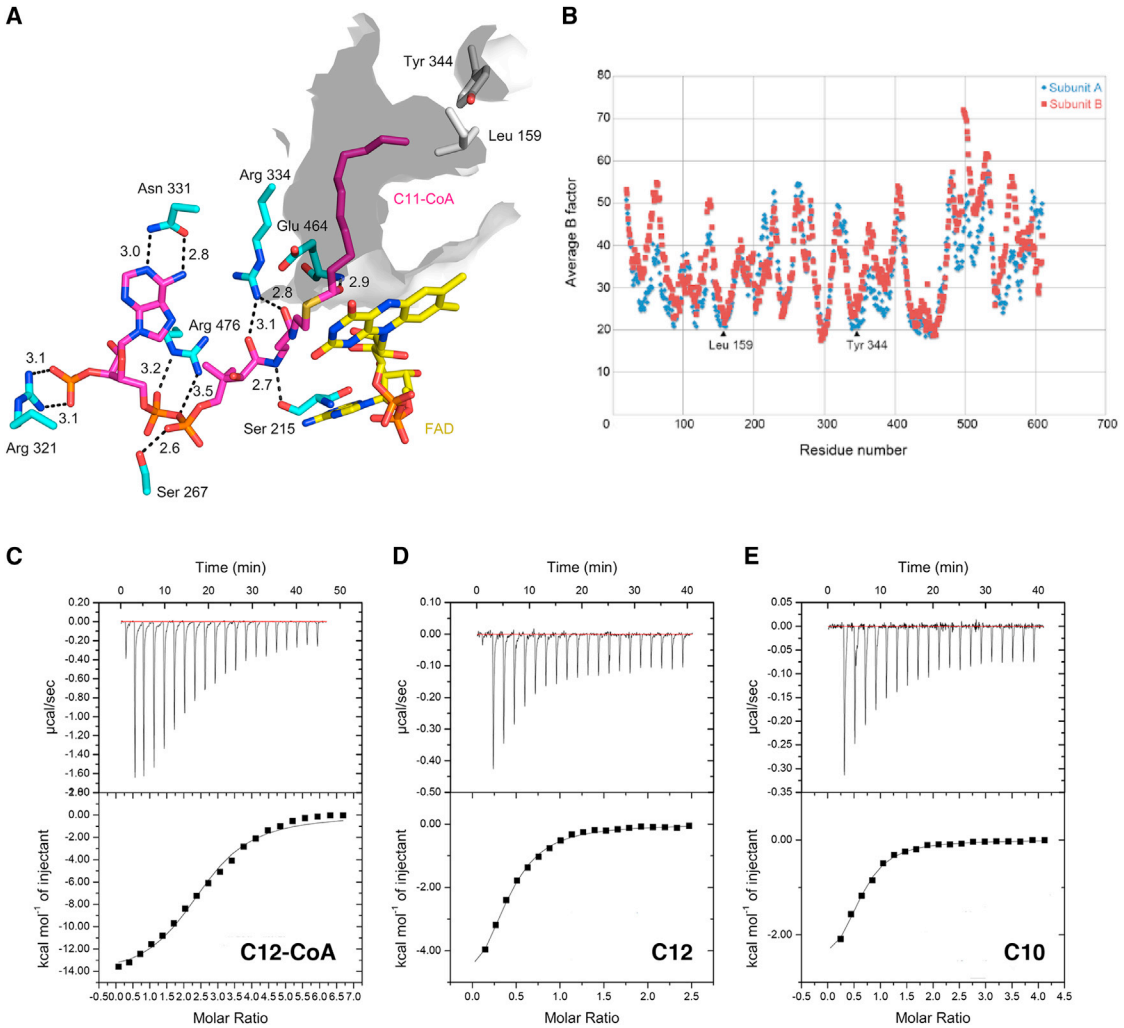


**Figure 5. Affinity and Selectivity of ACDH-11 Binding to Acyl-CoA Fatty Acids**

(A) Diagram of C11-CoA interactions with ACDH-11. Arg 321, Asn 331, and Arg 476 form six hydrogen bonds with the CoA moiety; these six bonds are not in other ACDH structures (see Figures S5 and S6). The hydrogen bonds formed by Ser 215, Ser 267, and Arg 334, which are found in SCAD or MCAD (see Figure S6), are also shown. The carbonyl oxygen of the thioester of C11-CoA is hydrogen-bonded with the amino nitrogen of Glu 464, a conserved catalytic residue in ACDHs, indicating a sandwich-like conformation comprising Glu 464, the thioester carbonyl, and the flavin ring. The cavity (gray) depth is limited by Tyr 344 and Leu 159.

(B) Plot of Temperature-B factor versus residue number of ACDH-11 showing that both Leu 159 and Tyr 344 have low Temperature B-factors and indicating the low mobility of these two residues.

(C–E) Isothermal titration calorimetry (ITC) measurements of C12-CoA (C), C12 (D), and C10 (E) binding strengths to ACDH-11. The profiles of the ITC binding data with the baseline subtracted are shown at the top. The peak-integrated and concentration-normalized enthalpy changes versus the molar ratios of ligands over the ACDH-11 protein are plotted at the bottom.

constants for C10, C12, and C12-CoA binding to purified ACDH-11 are 21.3 ± 2.6 μM, 10.3 ± 2.4 μM, and 5.2 ± 1.3 μM, respectively, and no significant binding was detected for C8 (Figures S5G and S5H). These biochemical results demonstrate the selectivity of ACDH-11 for fatty acids with chain lengths from C10 to C12, fully consistent with our conclusions based on structural observations. We obtained the structure of the complex without having added any ligand supplement during crystal growth, as C11-CoA presumably was tightly sequestered by ACDH-11 during the step of protein expression in *E. coli*.

## ACDH-11, C11/C12-Fatty Acids, and NHR-49 Act in a Pathway to Drive Heat Adaptation

The strong and selective binding of C11/C12-chain fatty acids to ACDH-11 indicated by the crystal structure of ACDH-11 could explain the functional specificity of ACDH-11 in regulating *fat-7* expression and heat adaptation. Specifically, we hypothesize that heat-induced ACDH-11 sequesters intracellular C11/C12-chain fatty acids, which are required for activating nuclear *fat-7* expression through fatty acid-regulated transcription factors.

To test this hypothesis, we examined whether supplementing *C. elegans* with exogenous fatty acids of various lengths could

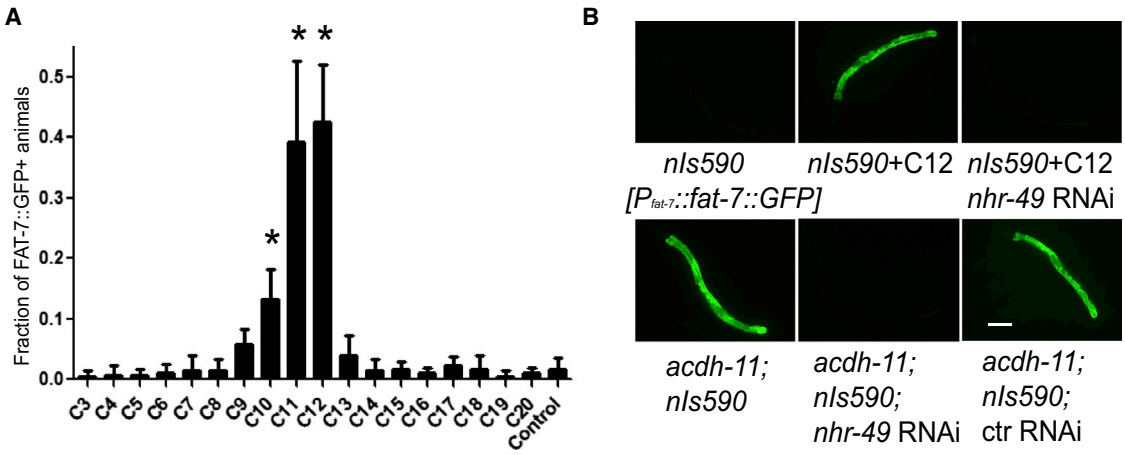


**Figure 6. ACDH-11 Acts through a Fatty Acid-Mediated Transcriptional Pathway**

(A) Fractions of otherwise wild-type adults carrying the $P_{fat\text{-}7}$*::fat-7::GFP* reporter *nIs590* in which this reporter was activated by various fatty acids. Control, animals treated with only the fatty acid-salt solvent M9 buffer. $p < 0.01$ ($n = 100$ for each of four independent experiments).

(B) Representative Nomarski and GFP fluorescence micrographs of wild-type transgenic adults showing that RNAi against *nhr-49* blocks activation of *nIs590* reporters by C11/C12 or *acdh-11* mutations. Control, animals with an RNAi vector L4440. Scale bar, 100 μm.

stimulate *fat-7* expression. We tested effects of a fatty acid series from C3 to C20 on the expression of $P_{fat\text{-}7}$*::fat-7::GFP*. At 25°C, this reporter was turned off (Figure 6A). Most of the fatty acids had no significant effects on FAT-7::GFP expression. By contrast, C10, C11, and C12 activated reporter expression in markedly higher fractions of the animals (Figure 6A). The activity of C10 was lower than that of C11 and C12. *fat-7* is a known transcriptional target of NHR-49 (Pathare et al., 2012; Van Gilst et al., 2005), a *C. elegans* homolog of the mammalian transcription factors PPARα and HNF4α, which are known to bind fatty acids, including C12 (Dhe-Paganon et al., 2002). We found that *nhr-49* RNAi eliminated the effect of C11 or C12 in activating FAT-7::GFP (Figure 6B). *nhr-49* RNAi or mutations also completely blocked overexpression of FAT-7::GFP in *acdh-11* mutants (Figures 6B and S7A). NHR-49 shares high sequence identity (37% amino acid residues; Figures S7B and S7C) with HNF4α (Dhe-Paganon et al., 2002), suggesting that NHR-49 likely exhibits a fatty acid-binding pocket that can accommodate C11/C12 fatty acids. These results indicate that C11/C12 requires NHR-49 to activate *fat-7* expression and that ACDH-11 sequesters C11/C12 fatty acids and thereby prevents them from activating nuclear *fat-7* expression.

## DISCUSSION

Based on our observations, we propose a model for how ACDH-11 regulates *C. elegans* heat adaptation (Figure 7). Under cold conditions (e.g., 15°C), intracellular C11/C12 fatty acids promote *fat-7* expression via fatty acid-regulated nuclear receptors (e.g., NHR-49). Upregulation of *fat-7* promotes lipid desaturation and thus membrane fluidity, which is an adaptation to cold. As a PAQR-related transmembrane protein with a ceramidase or phospholipase-like domain (Pei et al., 2011), EGL-25 likely acts to increase levels of C11/C12 and hence promote signaling in cooperation with NHR-49 (Svensk et al., 2013) and other NHRs (Brock et al., 2006; Pathare et al., 2012) for cold adaptation. Our data suggest that intracellular C11/C12 fatty acids activate *fat-7* expression via NHRs, which likely require lipid-transporting proteins to transduce C11/C12 fatty acid signals into the nucleus; however, we do not exclude the possibility that C11/C12 fatty acids might be further metabolized or processed to indirectly modulate NHR activation. In the cold, *acdh-11* is expressed at low levels and has little or no function.

Under heat conditions (e.g., 25°C), *acdh-11* is transcriptionally upregulated, and elevated levels of the ACDH-11 protein sequester intracellular C11/C12, preventing downstream NHR activation and consequent *fat-7* expression, thereby promoting lipid saturation and membrane rigidity in response to heat. Upstream sensors and mediators of this heat-induced *acdh-11* upregulation remain to be identified. At high temperature, in both wild-type animals and *egl-25* mutants C11/C12 is sequestered by ACDH-11, resulting in normal adaption to heat. By contrast, in *egl-25*; *acdh-11* double mutants as well as in *acdh-11* single mutants, C11/C12 is not sequestered by ACDH-11, and its consequent higher levels drive *fat-7* expression (although *fat-7* expression requires NHR-49, our data do not preclude the possibility that ACDH-11 sequestration of C11/C12 also prevents the activation of other NHRs). The resulting membrane lipid desaturation causes excessive membrane fluidity and thus a failure to adapt to heat. The genetic epistatic interactions among *egl-25*, *acdh-11*, and *nhr-49*, the high penetrance of their corresponding mutant phenotypes (Figures 1 and S7A) as well as mechanistic insights from the ACDH-11 structure together strongly support this model.

In both prokaryotic and eukaryotic cells, SCD fatty acid desaturases catalyze the limiting step of fatty acid desaturation and mediate HVA by maintaining optimal ranges of membrane fluidity in response to temperature shifts (Cossins and Prosser, 1978; de Mendoza, 2014; Flowers and Ntambi, 2008; Sinensky, 1974; Zhang and Rock, 2008). Bacterial two-component

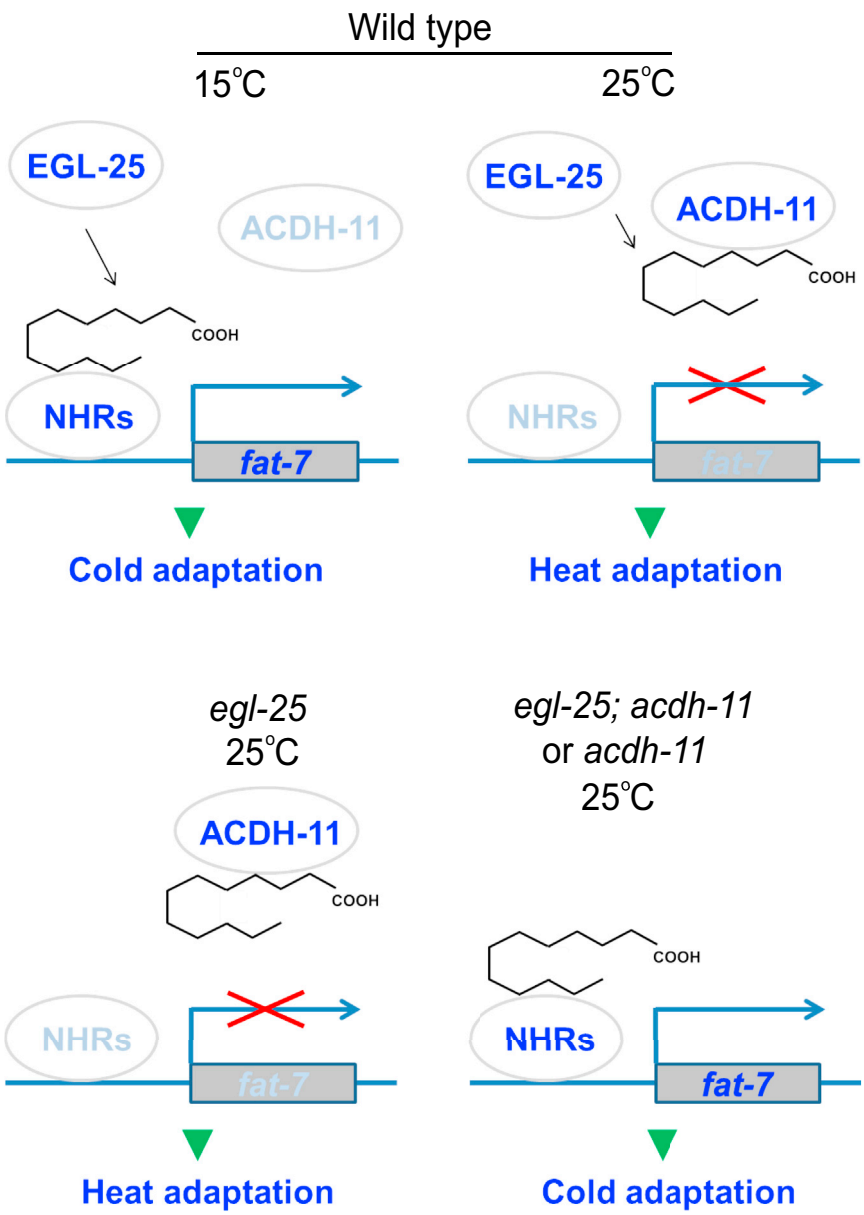


**Figure 7. Model for ACDH-11 Function**

Model showing proposed mechanism for how the ACDH-11 pathway mediates C11/C12 fatty acid signaling and heat adaptation. Heat upregulates ACDH-11, which prevents C11/C12 from activating NHRs and *fat-7* expression, leading to low levels of membrane lipid desaturation and reduced membrane fluidity for adaptation to heat (see text for details). Light blue indicates low protein activity or a low level of protein abundance. 15°C and 25°C represent low and high temperatures, respectively.
See also Figure S7.

systems, which are not present in eukaryotes, link membrane sensing of temperature shifts to nuclear transcription of desaturase genes for HVA (Aguilar et al., 2001; de Mendoza, 2014). Eukaryotic organisms, including warm-blooded animals, also exhibit HVA (Anderson et al., 1981; Cossins and Prosser, 1978; Shmeeda et al., 2002), a phenomenon far less studied and understood than bacterial HVA. Unlike systemic thermoregulation, eukaryotic HVA likely evolved as a mechanism to locally and cell-autonomously respond to temperature shifts. Cold temperature upregulates the plasma levels of adiponectin in humans (Imbeault et al., 2009), although roles of adiponectin and its receptors in HVA have not been explored. *C. elegans* SCDs and adiponectin receptor homologs have been proposed to regulate cold adaptation (Svensk et al., 2013; Svensson et al., 2011). Our findings support this hypothesis and further identify functional roles of ACDH-11 and C11/C12 fatty acids in the *egl-25* and *fat-7* pathway to control HVA in *C. elegans*. Unlike long-chain fatty acids that are well-known to mediate various cell signaling processes, sequestration of medium-chain C11/C12 fatty acids by ACDH-11 represents an unprecedented mode of fatty acid signaling. The novel pathway and mechanisms we have discovered provide a molecular basis for homeoviscous heat adaptation in *C. elegans*, shedding light on a long-standing mystery concerning a fundamental cell biological problem.

Mutations in human ACDH genes cause disorders of fatty acid oxidation that become life-threatening under fever or hyperthermia (Jank et al., 2014; O'Reilly et al., 2004; Zolkipli et al., 2011), with responses that are analogous to the vulnerability of *C. elegans acdh-11* mutants to heat. Although maintaining a sufficient diet is currently the standard-of-care management option to prevent symptoms of ACDH-deficiency in human patients, hyperthermia is a more significant independent risk factor than hypoglycemia (Rinaldo et al., 2002; Wolfe et al., 1993; Zolkipli et al., 2011). Our findings suggest that imbalance of lipid desaturation contributes to heat sensitivity of human ACDH-deficient patients and that therapeutic targeting of lipid desaturases might alleviate the thermo-sensitive syndrome of human ACDH-deficient patients. In addition, we found that ACDH-11 acts in a metabolic pathway to modulate activation of nuclear receptors by sequestering C11/C12 fatty acids, a plausibly widespread mechanism of controlling intracellular fatty acid signaling. Given that lipid metabolism and signaling are fundamentally similar between nematodes and other organisms (Ashrafi, 2007; Grevengoed et al., 2014; Holthuis and Menon, 2014; McKay et al., 2003; Nakamura and Nara, 2004; Srinivasan, 2015; Watts, 2009), we propose that the pathway and mechanisms we have

identified for *C. elegans* are evolutionarily conserved and modulate lipid metabolic homeostasis as well as thermal adaptation-associated physiological and pathological processes in other organisms, including humans.

## EXPERIMENTAL PROCEDURES

### EMS Mutagenesis, Genetic Screens, and Whole-Genome Sequencing

To screen for *egl-25* suppressors, we mutagenized *egl-25(n573)* mutants carrying the $P_{fat-7}$*::fat-7::GFP* transgene *nIs590* with ethyl methanesulfonate (EMS) and observed the F2 progeny using a dissecting microscope and GFP fluorescence at 20°C. We isolated suppressor mutants with restored expression of $P_{fat-7}$*::fat-7::GFP* in *egl-25* mutants. We mapped the suppressor mutations using standard genetic techniques based on polymorphic SNPs between the Bristol strain N2 and the Hawaiian strain CB4856 (Davis et al., 2005). We used whole-genome sequencing to identify the mutations; data analyses were performed as described (Sarin et al., 2008).

### Mutations and Strains

*C. elegans* strains were cultured as described (Brenner, 1974). The N2 Bristol strain (Brenner, 1974) was the reference wild-type strain, and the polymorphic Hawaiian strain CB4856 (Wicks et al., 2001) was used for genetic mapping and SNP analysis. Mutations used were as follows: LG I, *nhr-49(nr2041)* (Van Gilst et al., 2005); LG III, *egl-25(n573, gk395168, ok3136)* (Thompson et al., 2013; Trent et al., 1983), *acdh-11(n5655, n5657, n5661, n5876, n5877, n5878, n5879, n5880, gk753061)*; LG V, and *fat-7(wa36)* (Watts and Browse, 2000). *gk395168* and *gk753061* (molecular null, causing an L119-to-amber stop codon) were obtained from the Million Mutation Project and outcrossed six times (Thompson et al., 2013).

Transgenic strains were generated by germline transformation (Mello et al., 1991). Transgenic constructs were co-injected (at 10–50 ng/μl) with mCherry reporters, and lines of mCherry-positive animals were established. Gamma irradiation was used to generate integrated transgenes. Transgenic strains used were as follows: *nIs590[*$P_{fat-7}$*::fat-7::GFP]* (integrated from the extrachromosomal array *waEx15[*$P_{fat-7}$*::GFP + lin15(+)]*) (Brock et al., 2006); *nIs616[egl-25(+);* $P_{unc-54}$*::mCherry]; nIs677[*$P_{acdh-11}$*::GFP;* $P_{unc-54}$*::mCherry]; nEx2270 [acdh-11(+);*$P_{unc-54}$*::mCherry]*.

### Protein Purification, Structure Determination, Model Building, and Refinement

Protein was expressed and purified as described (Li et al., 2010). Briefly, the *acdh-11* gene was amplified and cloned into the expression vector pEXS-DH (derived from pET-22b, Novagen). 8xHis-tagged ACDH-11 was expressed in the *E. coli* strain BL21 (DE3) and isolated from the cell lysate by Ni2+-NTA (QIAGEN) affinity chromatography. ACDH-11 was further purified using ion exchange chromatography (RESOURCE S column, GE Healthcare) and size exclusion chromatography (Superdex 200 100/300 GL Column, GE Healthcare). For crystallization, ACDH-11 was concentrated to 12 mg/ml in 20 mM Tris pH 8.0, 150 mM NaCl. Large yellow crystals grew in 100 mM Tris pH 8.0, 200 mM magnesium formate, and 13% PEG 3350 through sitting-drop vapor diffusion at 16°C.

Immediately prior to data collection, the ACDH-11 crystal was quickly soaked in cryoprotectant solution (13% PEG 3350 and 20% glycerol) and flash-cooled at 100°K in a stream of nitrogen gas. The high-resolution diffraction data set for the complex structure was collected on beamline BL5A of the Photon Factory (KEK). The diffraction data set for the apo structure was collected on beamline BL17U of Shanghai Synchrotron Radiation Facility (SSRF). The structure of ACDH-11 was resolved by molecular replacement using the program Phaser (McCoy et al., 2007). ACDH-11 shares 30% sequence identity with *E. coli* AidB (Bowles et al., 2008), and the refined coordinates of AidB were used to construct the search model. The programs Coot (Emsley and Cowtan, 2004) and Refmac5 (Murshudov et al., 1997) were used for manual model building and refinement. The difference-Fourier map exhibited long and continuous electron densities corresponding to the FAD co-factor acyl-CoA. The length of acyl-chain was determined according to the electron density. C11-CoA was assigned because of its best RSCC (real space correlation coefficient, see Figures 5E and 5F). The statistics of data collection and structural refinement are summarized in Table S1.

The coordinates for the final refined model were deposited in the Protein Data Bank (PDB) with the accession number 4Y9J for the C11-CoA bound structure and 4Y9L for the C11-CoA free structure of ACDH-11.

### Isothermal Titration Calorimetry

Isothermal titration calorimetry (ITC) measurements were performed with a MicroCal iTC-200 titration micro-calorimeter (GE Healthcare) at 25°C. The sample cell was filled with ACDH-11 (25 μM in 20 mM MES, pH 6.5, and 10% glycerol). ACDH-11 concentration was determined by the bicinchoninic acid (BCA) method. The free fatty acids C8, C10, C12 and C14, and C12-CoA (800 μM) prepared in the same buffer were injected into the sample cell in 2-min time intervals. Twenty injections in total were conducted within 40 min. The reaction solution contained 1% DMSO to increase the solubility of fatty acids. As negative control, the ligands were titrated into the buffer without ACDH-11 proteins. All experiments were repeated five times. The data were processed using the Origin software (Version 7.0).

### Gene Expression Analyses

For qPCR and RNA-Seq experiments, total RNA from age-synchronized young adult (24 hr post-L4) hermaphrodites (200 in total, picked manually) was prepared using TissueRuptor and the RNeasy Mini kit (QIAGEN). Reverse transcription was performed by SuperScript III, and quantitative PCR was performed using Applied Biosystems Real-Time PCR Instruments. The specific intron-spanning primer sequences used were: *act-3* forward: TCCATCATGAAGTGCGACAT; *act-3* reverse: TAGATCCTCCGATCCAGACG; *fat-7* forward: ACGAGCTTGTCTTCCATGCT; *fat-7* reverse: AGCCCATTCAATGATGTCGT; *acdh-11* forward: TTGATCCATTTGTTCGGAGA; *acdh-11* reverse: GGTGGCTAGCTTGTGCTTTC. RNA-seq was performed by the Illumina TruSeq chemistry, and data were analyzed using standard protocols (Trapnell et al., 2010).

Nomarski and GFP fluorescence images of anesthetized *C. elegans* were obtained using an Axioskop II (Zeiss) compound microscope and OpenLab software (Agilent). The fraction of FAT-7::GFP-positive animals observed was quantified by counting animals using a dissecting microscope equipped for the detection of GFP fluorescence.

## SUPPLEMENTAL INFORMATION

Supplemental Information includes Supplemental Experimental Procedures, seven figures, and one table and can be found with this article online at http://dx.doi.org/10.1016/j.cell.2015.04.026.

## AUTHOR CONTRIBUTIONS

H.R.H. supervised the project. D.K.M. initiated the project and with Z.L., A.L., F.S., S.C., M.R., and R.M. F.S. designed and performed the experiments. Z.L. solved the ACDH-11 structures. F.S. and Z.L. performed the structural analysis. All authors contributed to data analysis, interpretation, and manuscript preparation.

## ACKNOWLEDGMENTS

We thank E. Boyden, A. Fire, Y. Iino, and M. Pilon for reagents and the *Caenorhabditis* Genetics Center and the Million Mutation Project for strains, and M. Bai, N. Bhatla, S. Luo, R. Vozdek, T. Wang, and J. Ward for comments on the manuscript. H.R.H. is an Investigator of the Howard Hughes Medical Institute and the David H. Koch Professor of Biology at MIT. This work was supported by NIH grants GM24663 (H.R.H.) and K99HL116654 (D.K.M.), Chinese Ministry of Science and Technology grant 2011CB910301 and 2011CB910901 (F.S.), German Research Foundation grant ME2056/3-1 (R.M.), Damon Runyon Fellowship DRG-2117-12 (S.C.), and Helen Hay Whitney and Charles King Trust postdoctoral fellowships (D.K.M.).

Received: November 6, 2014
Revised: February 26, 2015
Accepted: March 13, 2015
Published: May 14, 2015

## REFERENCES

Aguilar, P.S., Hernandez-Arriaga, A.M., Cybulski, L.E., Erazo, A.C., and de Mendoza, D. (2001). Molecular basis of thermosensing: a two-component signal transduction thermometer in *Bacillus subtilis*. EMBO J. *20*, 1681–1691.

Anderson, R.L., Minton, K.W., Li, G.C., and Hahn, G.M. (1981). Temperature-induced homeoviscous adaptation of Chinese hamster ovary cells. Biochim. Biophys. Acta *641*, 334–348.

Antebi, A. (2006). Nuclear hormone receptors in *C. elegans*. WormBook, 1–13.

Ashrafi, K. (2007). Obesity and the regulation of fat metabolism. WormBook, 1–20.

Atherton, H.J., Jones, O.A., Malik, S., Miska, E.A., and Griffin, J.L. (2008). A comparative metabolomic study of NHR-49 in *Caenorhabditis elegans* and PPAR-alpha in the mouse. FEBS Lett. *582*, 1661–1666.

Baird, N.A., Douglas, P.M., Simic, M.S., Grant, A.R., Moresco, J.J., Wolff, S.C., Yates, J.R., 3rd, Manning, G., and Dillin, A. (2014). HSF-1-mediated cytoskeletal integrity determines thermotolerance and life span. Science *346*, 360–363.

Battaile, K.P., Molin-Case, J., Paschke, R., Wang, M., Bennett, D., Vockley, J., and Kim, J.J. (2002). Crystal structure of rat short chain acyl-CoA dehydrogenase complexed with acetoacetyl-CoA: comparison with other acyl-CoA dehydrogenases. J. Biol. Chem. *277*, 12200–12207.

Bowles, T., Metz, A.H., O'Quin, J., Wawrzak, Z., and Eichman, B.F. (2008). Structure and DNA binding of alkylation response protein AidB. Proc. Natl. Acad. Sci. USA *105*, 15299–15304.

Brenner, S. (1974). The genetics of *Caenorhabditis elegans*. Genetics *77*, 71–94.

Brock, T.J., Browse, J., and Watts, J.L. (2006). Genetic regulation of unsaturated fatty acid composition in *C. elegans*. PLoS Genet. *2*, e108.

Cossins, A.R., and Prosser, C.L. (1978). Evolutionary adaptation of membranes to temperature. Proc. Natl. Acad. Sci. USA *75*, 2040–2043.

Davis, M.W., Hammarlund, M., Harrach, T., Hullett, P., Olsen, S., and Jorgensen, E.M. (2005). Rapid single nucleotide polymorphism mapping in *C. elegans*. BMC Genomics *6*, 118.

de Mendoza, D. (2014). Temperature sensing by membranes. Annu. Rev. Microbiol. *68*, 101–116.

Dhe-Paganon, S., Duda, K., Iwamoto, M., Chi, Y.I., and Shoelson, S.E. (2002). Crystal structure of the HNF4 alpha ligand binding domain in complex with endogenous fatty acid ligand. J. Biol. Chem. *277*, 37973–37976.

Emsley, P., and Cowtan, K. (2004). Coot: model-building tools for molecular graphics. Acta Crystallogr. D Biol. Crystallogr. *60*, 2126–2132.

Evans, R.M., and Mangelsdorf, D.J. (2014). Nuclear receptors, RXR, and the Big Bang. Cell *157*, 255–266.

Flowers, M.T., and Ntambi, J.M. (2008). Role of stearoyl-coenzyme A desaturase in regulating lipid metabolism. Curr. Opin. Lipidol. *19*, 248–256.

Garrity, P.A., Goodman, M.B., Samuel, A.D., and Sengupta, P. (2010). Running hot and cold: behavioral strategies, neural circuits, and the molecular machinery for thermotaxis in *C. elegans* and Drosophila. Genes Dev. *24*, 2365–2382.

Grevengoed, T.J., Klett, E.L., and Coleman, R.A. (2014). Acyl-CoA metabolism and partitioning. Annu. Rev. Nutr. *34*, 1–30.

Hedgecock, E.M., and Russell, R.L. (1975). Normal and mutant thermotaxis in the nematode *Caenorhabditis elegans*. Proc. Natl. Acad. Sci. USA *72*, 4061–4065.

Holthuis, J.C., and Menon, A.K. (2014). Lipid landscapes and pipelines in membrane homeostasis. Nature *510*, 48–57.

Imbeault, P., Dépault, I., and Haman, F. (2009). Cold exposure increases adiponectin levels in men. Metabolism *58*, 552–559.

Jank, J.M., Maier, E.M., Reiß, D.D., Haslbeck, M., Kemter, K.F., Truger, M.S., Sommerhoff, C.P., Ferdinandusse, S., Wanders, R.J., Gersting, S.W., et al. (2014). The domain-specific and temperature-dependent protein misfolding phenotype of variant medium-chain acyl-CoA dehydrogenase. PLoS ONE *9*, e93852.

Jordt, S.E., McKemy, D.D., and Julius, D. (2003). Lessons from peppers and peppermint: the molecular logic of thermosensation. Curr. Opin. Neurobiol. *13*, 487–492.

Kim, J.J., Wang, M., and Paschke, R. (1993). Crystal structures of medium-chain acyl-CoA dehydrogenase from pig liver mitochondria with and without substrate. Proc. Natl. Acad. Sci. USA *90*, 7523–7527.

Kourtis, N., Nikoletopoulou, V., and Tavernarakis, N. (2012). Small heat-shock proteins protect from heat-stroke-associated neurodegeneration. Nature *490*, 213–218.

Li, Z., Zhai, Y., Fang, J., Zhou, Q., Geng, Y., and Sun, F. (2010). Purification, crystallization and preliminary crystallographic analysis of very-long-chain acyl-CoA dehydrogenase from *Caenorhabditis elegans*. Acta Crystallogr. Sect. F Struct. Biol. Cryst. Commun. *66*, 426–430.

Lyman, G.H., Preisler, H.D., and Papahadjopoulos, D. (1976). Membrane action of DMSO and other chemical inducers of Friend leukaemic cell differentiation. Nature *262*, 361–363.

Ma, D.K., Vozdek, R., Bhatla, N., and Horvitz, H.R. (2012). CYSL-1 interacts with the O2-sensing hydroxylase EGL-9 to promote H2S-modulated hypoxia-induced behavioral plasticity in C. elegans. Neuron *73*, 925–940.

Ma, D.K., Rothe, M., Zheng, S., Bhatla, N., Pender, C.L., Menzel, R., and Horvitz, H.R. (2013). Cytochrome P450 drives a HIF-regulated behavioral response to reoxygenation by *C. elegans*. Science *341*, 554–558.

McAndrew, R.P., Wang, Y., Mohsen, A.W., He, M., Vockley, J., and Kim, J.J. (2008). Structural basis for substrate fatty acyl chain specificity: crystal structure of human very-long-chain acyl-CoA dehydrogenase. J. Biol. Chem. *283*, 9435–9443.

McCoy, A.J., Grosse-Kunstleve, R.W., Adams, P.D., Winn, M.D., Storoni, L.C., and Read, R.J. (2007). Phaser crystallographic software. J. Appl. Cryst. *40*, 658–674.

McKay, R.M., McKay, J.P., Avery, L., and Graff, J.M. (2003). *C elegans*: a model for exploring the genetics of fat storage. Dev. Cell *4*, 131–142.

Mello, C.C., Kramer, J.M., Stinchcomb, D., and Ambros, V. (1991). Efficient gene transfer in *C.elegans*: extrachromosomal maintenance and integration of transforming sequences. EMBO J. *10*, 3959–3970.

Mori, I., and Ohshima, Y. (1995). Neural regulation of thermotaxis in *Caenorhabditis elegans*. Nature *376*, 344–348.

Mullaney, B.C., Blind, R.D., Lemieux, G.A., Perez, C.L., Elle, I.C., Faergeman, N.J., Van Gilst, M.R., Ingraham, H.A., and Ashrafi, K. (2010). Regulation of *C. elegans* fat uptake and storage by acyl-CoA synthase-3 is dependent on NR5A family nuclear hormone receptor nhr-25. Cell Metab. *12*, 398–410.

Murray, P., Hayward, S.A., Govan, G.G., Gracey, A.Y., and Cossins, A.R. (2007). An explicit test of the phospholipid saturation hypothesis of acquired cold tolerance in *Caenorhabditis elegans*. Proc. Natl. Acad. Sci. USA *104*, 5489–5494.

Murshudov, G.N., Vagin, A.A., and Dodson, E.J. (1997). Refinement of macromolecular structures by the maximum-likelihood method. Acta Crystallogr. D Biol. Crystallogr. *53*, 240–255.

Nakamura, M.T., and Nara, T.Y. (2004). Structure, function, and dietary regulation of delta6, delta5, and delta9 desaturases. Annu. Rev. Nutr. *24*, 345–376.

O'Reilly, L., Bross, P., Corydon, T.J., Olpin, S.E., Hansen, J., Kenney, J.M., McCandless, S.E., Frazier, D.M., Winter, V., Gregersen, N., et al. (2004). The Y42H mutation in medium-chain acyl-CoA dehydrogenase, which is prevalent in babies identified by MS/MS-based newborn screening, is temperature sensitive. Eur. J. Biochem. *271*, 4053–4063.

Owen, D.M., Rentero, C., Magenau, A., Abu-Siniyeh, A., and Gaus, K. (2012). Quantitative imaging of membrane lipid order in cells and organisms. Nat. Protoc. *7*, 24–35.

Pathare, P.P., Lin, A., Bornfeldt, K.E., Taubert, S., and Van Gilst, M.R. (2012). Coordinate regulation of lipid metabolism by novel nuclear receptor partnerships. PLoS Genet. *8*, e1002645.

Pei, J., Millay, D.P., Olson, E.N., and Grishin, N.V. (2011). CREST—a large and diverse superfamily of putative transmembrane hydrolases. Biol. Direct *6*, 37.

Rinaldo, P., Matern, D., and Bennett, M.J. (2002). Fatty acid oxidation disorders. Annu. Rev. Physiol. *64*, 477–502.

Sangwan, V., Foulds, I., Singh, J., and Dhindsa, R.S. (2001). Cold-activation of Brassica napus BN115 promoter is mediated by structural changes in membranes and cytoskeleton, and requires Ca2+ influx. Plant J. *27*, 1–12.

Sarin, S., Prabhu, S., O'Meara, M.M., Pe'er, I., and Hobert, O. (2008). *Caenorhabditis elegans* mutant allele identification by whole-genome sequencing. Nat. Methods *5*, 865–867.

Sengupta, P., and Garrity, P. (2013). Sensing temperature. Curr. Biol. *23*, R304–R307.

Shmeeda, H., Kaspler, P., Shleyer, J., Honen, R., Horowitz, M., and Barenholz, Y. (2002). Heat acclimation in rats: modulation via lipid polyunsaturation. Am. J. Physiol. Regul. Integr. Comp. Physiol. *283*, R389–R399.

Sinensky, M. (1974). Homeoviscous adaptation—a homeostatic process that regulates the viscosity of membrane lipids in *Escherichia coli*. Proc. Natl. Acad. Sci. USA *71*, 522–525.

Srinivasan, S. (2015). Regulation of body fat in Caenorhabditis elegans. Annu. Rev. Physiol. *77*, 161–178.

Svensk, E., Ståhlman, M., Andersson, C.H., Johansson, M., Borén, J., and Pilon, M. (2013). PAQR-2 regulates fatty acid desaturation during cold adaptation in *C. elegans*. PLoS Genet. *9*, e1003801.

Svensson, E., Olsen, L., Mörck, C., Brackmann, C., Enejder, A., Faergeman, N.J., and Pilon, M. (2011). The adiponectin receptor homologs in *C. elegans* promote energy utilization and homeostasis. PLoS ONE *6*, e21343.

Thompson, O., Edgley, M., Strasbourger, P., Flibotte, S., Ewing, B., Adair, R., Au, V., Chaudhry, I., Fernando, L., Hutter, H., et al. (2013). The million mutation project: a new approach to genetics in *Caenorhabditis elegans*. Genome Res. *23*, 1749–1762.

Trapnell, C., Williams, B.A., Pertea, G., Mortazavi, A., Kwan, G., van Baren, M.J., Salzberg, S.L., Wold, B.J., and Pachter, L. (2010). Transcript assembly and quantification by RNA-Seq reveals unannotated transcripts and isoform switching during cell differentiation. Nat. Biotechnol. *28*, 511–515.

Trent, C., Tsuing, N., and Horvitz, H.R. (1983). Egg-laying defective mutants of the nematode *Caenorhabditis elegans*. Genetics *104*, 619–647.

Van Gilst, M.R., Hadjivassiliou, H., Jolly, A., and Yamamoto, K.R. (2005). Nuclear hormone receptor NHR-49 controls fat consumption and fatty acid composition in *C. elegans*. PLoS Biol. *3*, e53.

van Oosten-Hawle, P., and Morimoto, R.I. (2014). Organismal proteostasis: role of cell-nonautonomous regulation and transcellular chaperone signaling. Genes Dev. *28*, 1533–1543.

van Oosten-Hawle, P., Porter, R.S., and Morimoto, R.I. (2013). Regulation of organismal proteostasis by transcellular chaperone signaling. Cell *153*, 1366–1378.

Watts, J.L. (2009). Fat synthesis and adiposity regulation in *Caenorhabditis elegans*. Trends Endocrinol. Metab. *20*, 58–65.

Watts, J.L., and Browse, J. (2000). A palmitoyl-CoA-specific delta9 fatty acid desaturase from *Caenorhabditis elegans*. Biochem. Biophys. Res. Commun. *272*, 263–269.

Wicks, S.R., Yeh, R.T., Gish, W.R., Waterston, R.H., and Plasterk, R.H. (2001). Rapid gene mapping in *Caenorhabditis elegans* using a high density polymorphism map. Nat. Genet. *28*, 160–164.

Woldeyes, R.A., Sivak, D.A., and Fraser, J.S. (2014). E pluribus unum, no more: from one crystal, many conformations. Curr. Opin. Struct. Biol. *28*, 56–62.

Wolfe, L., Jethva, R., Oglesbee, D., and Vockley, J. (1993). Short-chain Acyl-CoA dehydrogenase deficiency. In GeneReviews, R.A. Pagon, M.P. Adam, H.H. Ardinger, S.E. Wallace, A. Amemiya, L.J.H. Bean, T.D. Bird, C.R. Dolan, C.T. Fong, and R.J.H. Smith, et al., eds. (University of Washington, Seattle), Bookshelf ID: NBK63582, http://www.ncbi.nlm.nih.gov/books/NBK63582/.

Zhang, Y.M., and Rock, C.O. (2008). Membrane lipid homeostasis in bacteria. Nat. Rev. Microbiol. *6*, 222–233.

Zolkipli, Z., Pedersen, C.B., Lamhonwah, A.M., Gregersen, N., and Tein, I. (2011). Vulnerability to oxidative stress in vitro in pathophysiology of mitochondrial short-chain acyl-CoA dehydrogenase deficiency: response to antioxidants. PLoS ONE *6*, e17534.

Cell

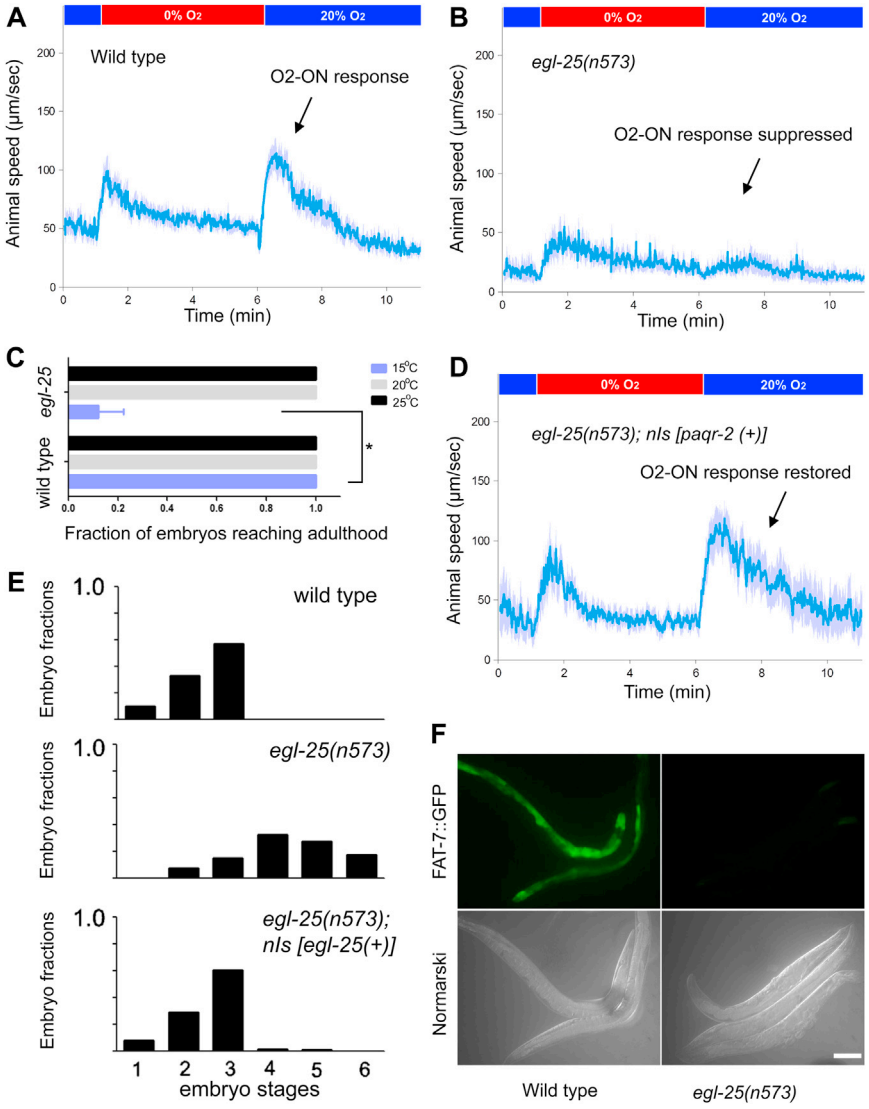


**Figure S1. Molecular Identification of *egl-25*, Related to Figure 1**

(A) Speed graph of wild-type animals, showing the normal O2-ON response (Ma et al., 2012).

(B) Speed graph of *egl-25(n573)* mutants, showing a defective O2-ON response.

(C) Fractions of embryos of wild-type or *egl-25(n573)* mutants that developed to adulthood at 15°C, 20°C and 25°C. $p < 0.01$ ($n = 20$ for each of five independent experiments).

(D) Speed graph of *egl-25(n573)* mutants, showing the rescue of the defective O2-ON response by an *egl-25*(+) transgene.

(E) Egg-laying defect of *egl-25(n573)* animals and rescue by an integrated *egl-25*(+) transgene. Fractions of the developmental stages of eggs (Ringstad and Horvitz, 2008) laid by young adults carrying the mutations indicated are shown. Late-stage embryos indicate an egg-laying defect.

(F) Fluorescence and Nomarski micrographs of otherwise wild-type *nIs590* transgenic adults showing expression of $P_{fat\text{-}7}$*::fat-7::GFP* in the wild-type but not in *egl-25*(*n573*) mutants. Scale bar, 100 µm.

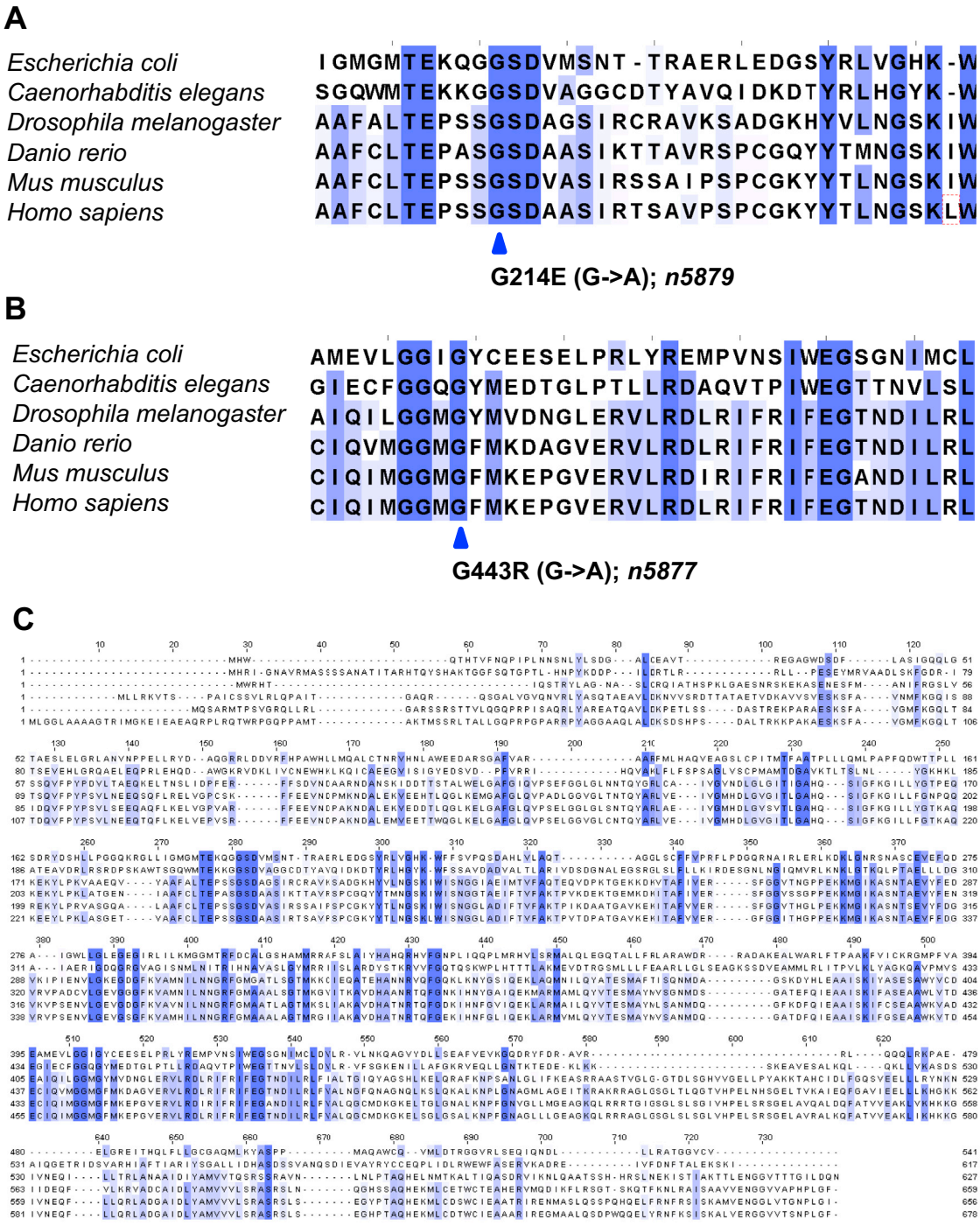


**Figure S2. Conservation of Residues Disrupted by Three *acdh-11* Mutations, Related to Figure 1**

Shown are sequence alignments of ACDH-11 homologs from *Escherichia coli* (AidB), *Drosophila melanogaster* (CG7461), *Danio rerio* (Acadvl), *Mus musculus* (Acadvl) and *Homo sapiens* (ACADVL). For clarity, two regions of these homologs containing the disrupted amino acid residues (A) and (B) and the full alignment (C) are shown separately. The three shades of blue indicate the degree of amino acid identity (deep blue > 80%; blue > 60%; light blue > 40%). Arrows, two completely conserved residues disrupted in *C. elegans* by the *acdh-11* mutations indicated.

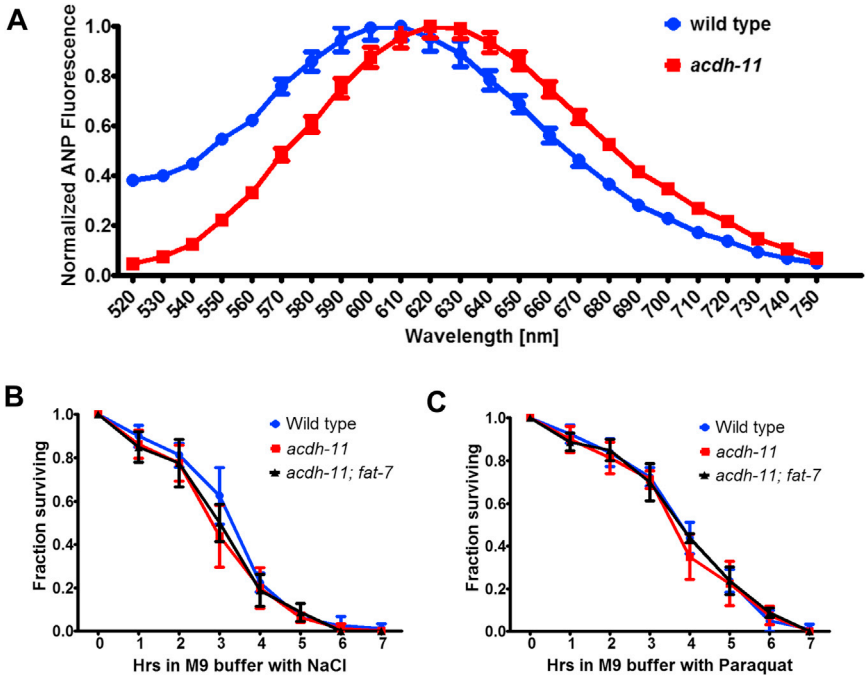


**Figure S3. Altered Membrane Fluidity, but Not Sensitivity to Stresses Other Than Heat, in *acdh-11* Mutants, Related to Figure 2**

(A) Di-4-ANEPPDHQ fluorescence spectra of age-synchronized (24 hr post-L4) young adult *C. elegans* populations in M9 buffer indicating relative extents of membrane fluidity of the wild-type type (blue) and *acdh-11* null mutants (red). $p < 0.01$ ($n = 4$ independent samples).

(B) Fractions of young adults (age-synchronized by bleaching, 24 hr post-L4) that survived high osmolality stress. Error bars, standard deviations ($n = 20$ for each of four independent experiments). Animals grown at 15°C were incubated in M9 buffer with 750 mM NaCl for indicated periods of time at 15°C. After 24 hr recovery, animals without pumping and that failed to respond to repeated touch were considered dead and counted for quantification.

(C) Fractions of young adults (age-synchronized by bleaching, 24 hr post-L4) that survived high oxidative stress. Error bars, standard deviations ($n = 20$ for each of four independent experiments). Animals grown at 15°C were incubated in M9 buffer with 300 mM Paraquat for indicated periods of time at 15°C. After 24 hr recovery, animals without pumping and that failed to respond to repeated touch were considered dead and counted for quantification.

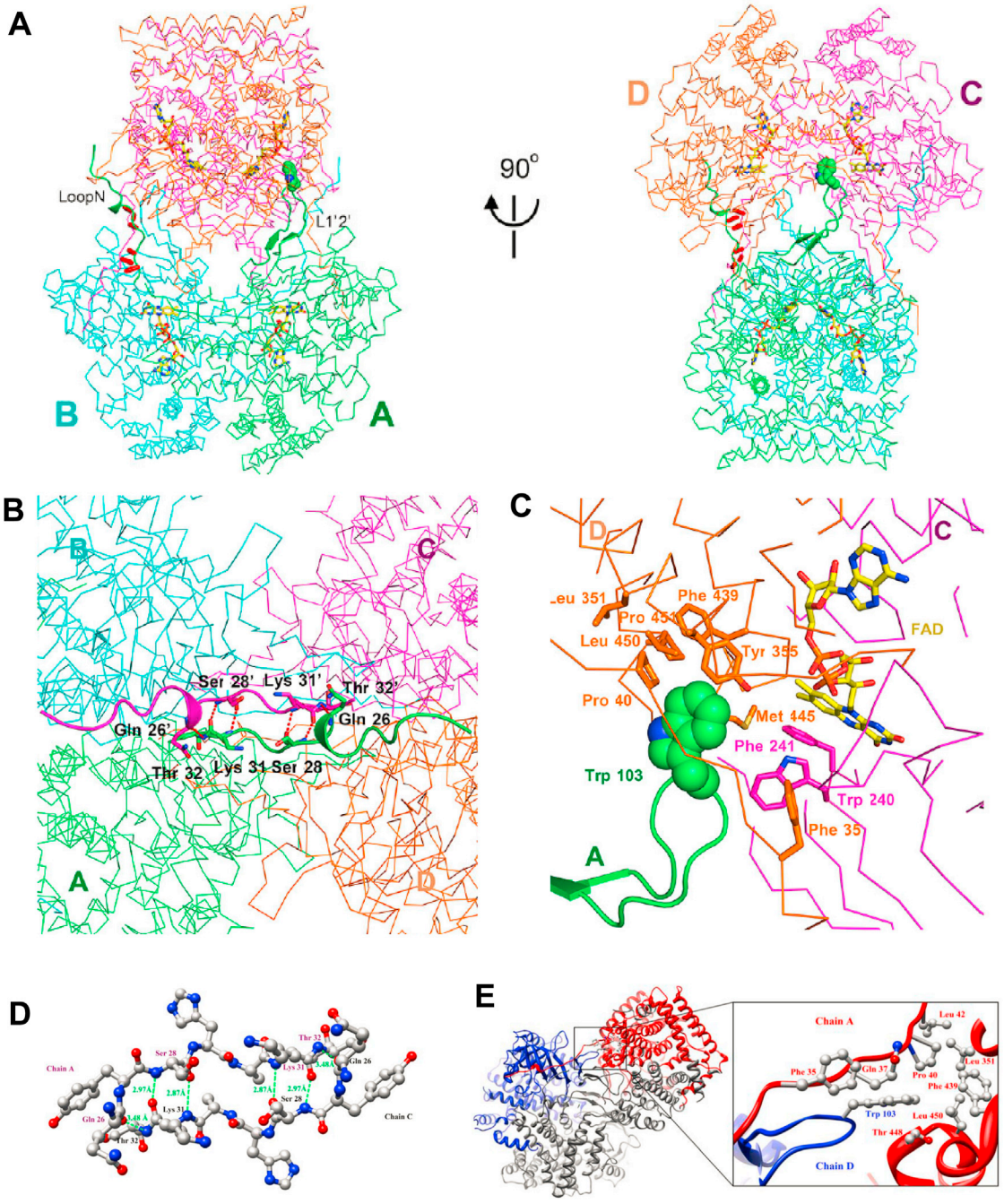


**Figure S4. ACDH-11 Tetramer Formation via N-Terminal Loop Interactions, Related to Figure 4**

(A) Ribbon representations of ACDH-11 tetramer showing that the dimer of dimers assembles at the subunit interfaces through the N-terminal loop (LoopN) and the L1'2′ loop from each subunit. The loopN and L1'2′ loop are shown for subunit A (green). The other three subunits are indicated in cyan (B), magenta (C), and orange (D).

(B) Interactions of the loopN regions between subunit A (green) and subunit C (magenta) illustrate the six hydrogen bonds formed via the four residues Gln 26, Ser 28, Lys 31 and Thr 32.

(C) Ribbon-stick representation showing a hydrophobic core on the AB/CD interface, consisting of Trp 103 of the subunit A L1'2′ loop, eight residues of subunit D (orange) and two residues of subunit C (magenta), and the FAD cofactor in subunit C (yellow stick).

(D) Ball-stick representation showing hydrogen bonds along loopN regions that facilitate ACDH-11 tetramer assembly.

(E) Ribbon-ball-stick representation showing hydrophobic interaction along loopN regions that facilitate ACDH-11 tetramer assembly.

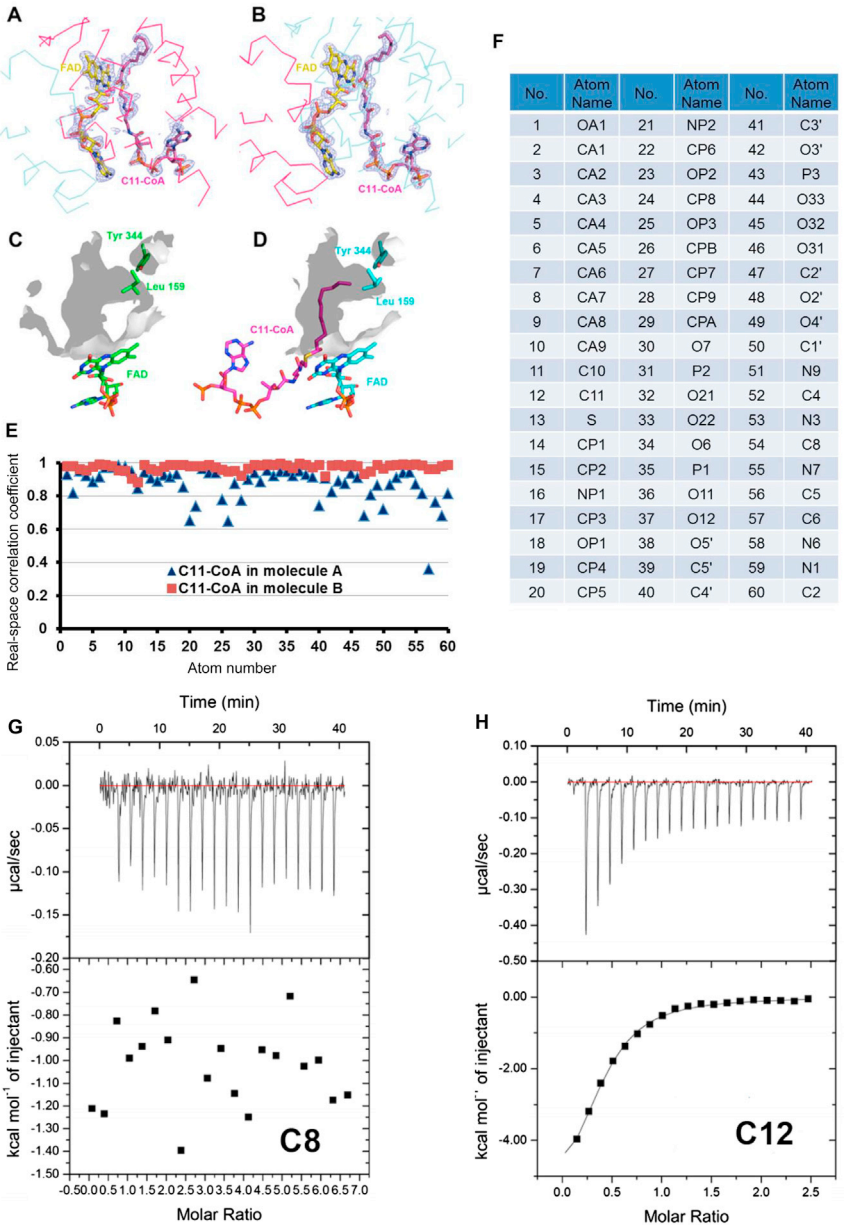


| No. | Atom Name | No. | Atom Name | No. | Atom Name |
|---|---|---|---|---|---|
| 1 | OA1 | 21 | NP2 | 41 | C3' |
| 2 | CA1 | 22 | CP6 | 42 | O3' |
| 3 | CA2 | 23 | OP2 | 43 | P3 |
| 4 | CA3 | 24 | CP8 | 44 | O33 |
| 5 | CA4 | 25 | OP3 | 45 | O32 |
| 6 | CA5 | 26 | CPB | 46 | O31 |
| 7 | CA6 | 27 | CP7 | 47 | C2' |
| 8 | CA7 | 28 | CP9 | 48 | O2' |
| 9 | CA8 | 29 | CPA | 49 | O4' |
| 10 | CA9 | 30 | O7 | 50 | C1' |
| 11 | C10 | 31 | P2 | 51 | N9 |
| 12 | C11 | 32 | O21 | 52 | C4 |
| 13 | S | 33 | O22 | 53 | N3 |
| 14 | CP1 | 34 | O6 | 54 | C8 |
| 15 | CP2 | 35 | P1 | 55 | N7 |
| 16 | NP1 | 36 | O11 | 56 | C5 |
| 17 | CP3 | 37 | O12 | 57 | C6 |
| 18 | OP1 | 38 | O5' | 58 | N6 |
| 19 | CP4 | 39 | C5' | 59 | N1 |
| 20 | CP5 | 40 | C4' | 60 | C2 |

**Figure S5. Further Structural Analysis of Fatty Acyl-CoA Binding to ACDH-11, Related to Figure 5**

(A and B) The ligand (FAD and C11-CoA) binding sites of ACDH-11 with mFo-DFc maximum-likelihood omit map for the ligands bound to chain A (pink) and for the ligands bound to chain B (cyan). The mFo-DFc maximum-likelihood omit map was calculated by REFMAC5 (Murshudov et al., 1997).

(C and D) Surface renderings (inside, light gray; outside, dark gray) of the binding cavities in ACDH-11 in the absence (C, apo-structure) and presence of C11-CoA (D, holo-structure). Leu 159 and Tyr 344 in the apo-structure exhibit the same confirmation as that in the holo-structure, indicating the low mobility of these two residues.

(E and F) The real-space correlation coefficient (RSCC) of the ligand C11-CoA against the electron density map is plotted versus the atom number (E). The detailed atom information for every atom number is shown in (F). The RSCC was computed using Phenix (Adams et al., 2010). (E) Isothermal titration calorimetry (ITC) results show no ACDH-11 binding to C8 fatty acids. The profiles of the ITC binding data with the baseline subtracted are shown at the top. The peak-integrated and concentration-normalized enthalpy changes versus the molar ratios of ligands over ACDH-11 are plotted at the bottom. (F) ITC results for ACDH-11 binding to C12 fatty acids are shown for comparison.

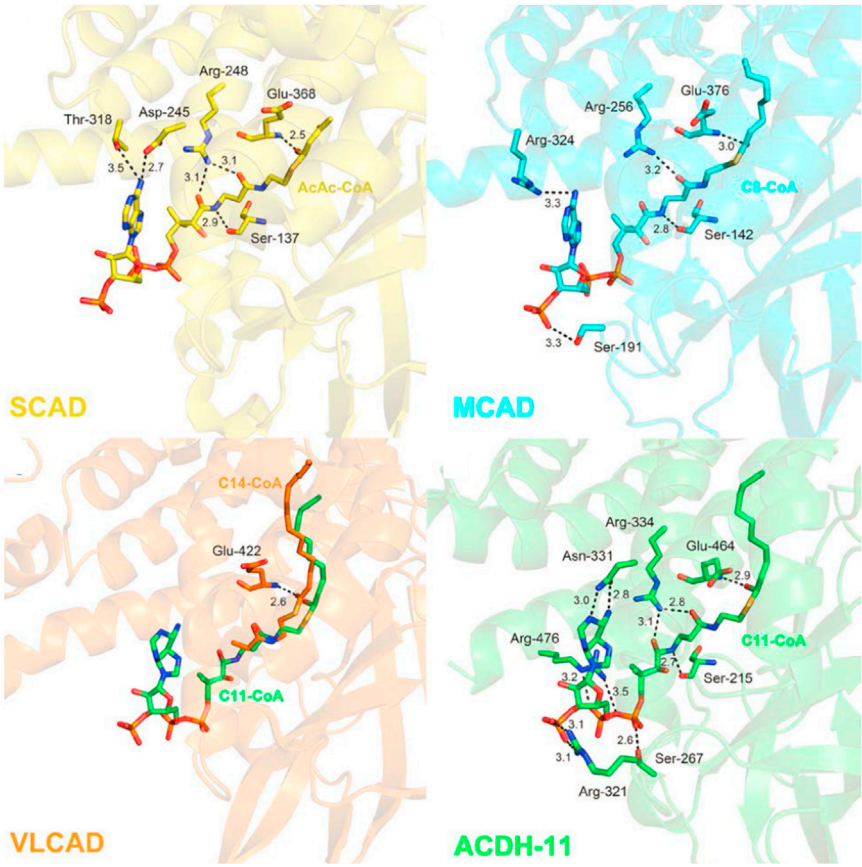


**Figure S6. Hydrogen Bond Interactions with Fatty Acid Substrates: ACDH-11 Compared with Other Structurally Characterized ACDHs, Related to Figure 5**

Structures of SCAD (yellow) (Battaile et al., 2002), MCAD (cyan) (Kim et al., 1993) and VLCAD (orange) (McAndrew et al., 2008) show that the CoA moiety of the substrate is less hydrogen-bonded as the substrate carbon length increases. SCAD, MCAD, and VLCAD have 5, 4 and 1 hydrogen bond(s), respectively, whereas ACDH-11 forms 11 hydrogen bonds, much more strongly stabilizing its interaction with the C11-CoA ligand. The hydrogen bonds formed via Ser 215 and Arg 334 in ACDH-11 were also observed in SCAD and MCAD. The hydrogen bond formed via Ser 267 was observed only in MCAD. The six hydrogen bonds formed by Arg 321, Asn 331 and Arg 476 were not observed in other ACDHs.

**A**

| Genotype | Fraction of FAT-7::GFP animals | Number of total animal examined |
|---|---|---|
| Wild type | 0.25 | 500 |
| *egl-25* | 0.00 | 500 |
| *acdh-11* | 1.00 | 500 |
| *nhr-49* | 0.00 | 500 |
| *egl-25; acdh-11* | 1.00 | 500 |
| *nhr-49; acdh-11* | 0.00 | 500 |

**B**

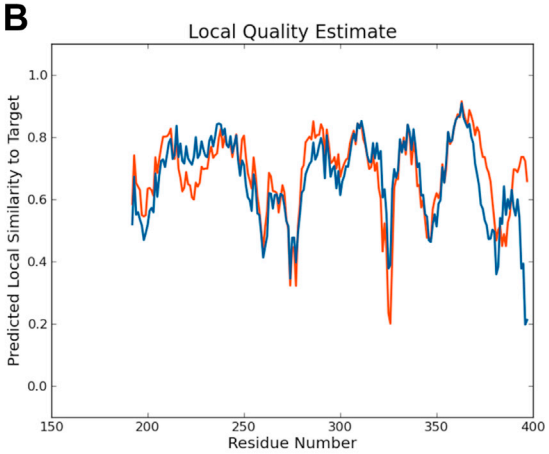


**C**

```
HNF4a       ------------------------------------SSYEDSSLPSINALLQAEVLSQQ
NHR-49      LNGTPFKKDRSPGYENGNSNGVGSNGMGQENMRTVPQSSSVIDALMEMEARVNQEMCNRY
                                                **   .:* .::* :: *: .:

HNF4a       ITSP-----ISGINGD----------------IRAKRIASITDVCESMKEQLLVLVEWAK
NHR-49      RRSQIFANGSGGSNGNDTDIQQGSDSGASAFAPPNRPCTTEVDLNEISRTTLLLMVEWAK
              *       .* **:                    :  :: .*: *  :  **::*****

HNF4a       YIPAFCELLLDDQVALLRAHAGEHLLLGATKRSMVFKDVLLLGNDYIVPRHCPELA----
NHR-49      TINPFMDLSMEDKIILLKNYAPQHLILMPAFRSPDTTRVCLFNNTYMTRDNNTDLNGFAA
             *  * :* ::*:: **: :* :**:*  : **   . * *: * *:.  .  :*

HNF4a       -EMSRVSIRILDELVLPFQELQIDDNEYACLKAIIFFDPDAKGLSDPGK--IKRLRSQVQ
NHR-49      FKTSNITPRVLDEIVWPMRQLQMREQEFVCLKALAFLHPEAKGLSNSSQIMIRDARNRVL
             : *.:: *:***:* *:::**: ::*:.****: *:.*:*****: .:  *:  *.:*

HNF4a       VSLEDYINDRQYDSR-GRFGELLLLLPTLQSITWQMIEQIQFIKLFGMAKIDNLLQEMLL
NHR-49      KALYAFILDQMPDDAPTRYGNILLLAPALKALTQLLIENMTLTKFFGLAEVDSLLSEFIL
             :*  :* *:  *.   *:*::*** *:*:::*  :**:: : *:**:*::*.**.*::*

HNF4a       G----GSASDAPHAHHPLHP----------------------------------------
NHR-49      DDINDHSTAPVSLQQHLSSPTTLPTNGVSPLNPAGSVGSVSSVSGITPTGMLSATLAAPL
                  *:: .   :*   *

HNF4a       --------------------
NHR-49      AIHPLQSQDSILNSEQNNHML
```

**Figure S7. Additional Evidence for a Role of NHR-49 in the EGL-25/ACDH-11 Pathway that Mediates C11/C12 Fatty Acid Signaling, Related to Figure 7**

(A) Table showing fractions of animals (n = 500 for each genotype) expressing FAT-7::GFP at 20°C in strains of the genotypes indicated.

(B) Local Similarity Plot showing the predicted similarity of NHR-49 to HNF4α at each of the aligned amino acid residues, generated by analysis using the SWISS-MODEL website http://swissmodel.expasy.org/.

(C) Alignment of NHR-49 and HNF4α showing 37% amino acid identity.

**Cell**

**Supplemental Information**

# Acyl-CoA Dehydrogenase Drives Heat Adaptation by Sequestering Fatty Acids

**Dengke K. Ma, Zhijie Li, Alice Y. Lu, Fang Sun, Sidi Chen, Michael Rothe, Ralph Menzel, Fei Sun, H. Robert Horvitz**

## Supplemental Experimental Procedures

### Di-4-ANEPPDHQ Assay, Fatty Acid Supplementation, and Abundance Measurements by LC-MS

Approximately 500 (per experiment) age-synchronized young adult (24 hrs post-L4) hermaphrodites grown at 20°C were collected and washed three times with M9 buffer. Di-4-ANEPPDHQ (Life Technologies) was dissolved in water and added to *C. elegans* samples in 50 µl M9 buffer at a final concentration 10 µg/ml. After 3 hrs of staining with gentle shaking at 20°C, samples were washed with M9 buffer three times and the fluorescence of samples in liquid was immediately measured using a SpectraMax Microplate Reader (Molecular Devices) with excitation at 475 nm and an emission sweep from 520 nm to 720 nm.

Fatty acid salts (Nu-Chek Prep, Inc.) were thoroughly dissolved in M9 buffer at 10 mg/ml, and 250 µl of each was added to an OP50-seeded NGM plate with uniform spreading of the fatty acid solution. Once the plates briefly dried, age-synchronized L4 hermaphrodites (cultured at 25°C to minimize baseline GFP expression) carrying the otherwise wild-type *nIs590* reporter were transferred to fatty acid-supplemented Petri plates. (We observed that several fatty acid salts were very toxic to *C. elegans* grown in liquid cultures and used Petri plates for this reason.) Animals were cultured at 25°C for 48 hrs before being examined with fluorescence microscopy. Endogenous levels of fatty acids were measured by LC-MS/MS, essentially as described (Ma et al., 2013).

### Stress-Sensitivity Assays of *C. elegans* Adults

Age-synchronized young adult (24 hrs post-L4) hermaphrodites grown at 15°C were transferred to specified conditions of stress (37°C on NGM Petri plates, 300 mM Paraquat in M9 buffer, or 750 mM NaCl in M9 buffer) (Rodriguez et al., 2013) for times ranging from 1 hr to 7 hrs (stress conditions were used that caused death of most animals over this period). Animals

were then allowed to recover at 15$^{o}$C on NGM Petri plates for 24 hrs. Animals without pumping and responses to repeated touch were considered dead and counted for quantification.

**Statistical Analyses**

Data were analyzed using GraphPad Prism Software and are presented as means ± standard deviations with p values calculated by the unpaired Student's t-test (comparisons between subjects) or one-way ANOVA (comparisons across more than two groups) and adjusted with the Bonferroni's correction. At least four biological replicates were used. For the O2-ON response, one-sided unpaired t-tests were used to compare the mean speeds of all animals within 120 seconds before or after oxygen restoration (Ma et al., 2012). Fisher's exact tests were used to analyze egg-laying behavioral data to compare the distributions of the six categories of embryos from the wild type and various mutants.

## Table S1. Crystallography Data Collection and Refinement Statistics, Related to Figure 4 and Experimental Procedures

Data collection

| | ACDH-11 w/ C11-CoA | ACDH-11 w/o C11-CoA |
|---|---|---|
| Space group | C2 | C2 |
| Unit cell parameters (Å, °) | a=138.6, b=116.7, c=115.3, α=γ=90.0, β=124.0 | a=137.9 , b=113.4, c=113.9 α=γ=90.0, β=124.0 |
| Wavelength (Å) | 1.00000 | 0.99985 |
| Resolution range (Å) | 50-1.80 (1.83-1.80)† | 50-2.27 (2.31-2.27)† |
| Completeness (%) | 99.8 (100) † | 98.9 (83.6) † |
| Redundancy | 7.5 (7.3) † | 7.2 (4.5) † |
| $R_{merge}$† (%) | 6.1 (78.0) † | 11.0 (39.4) † |
| Average I/σ (I) | 11.4 (2.2) † | 11.6 (4.1) † |
| Total reflections | 1052727 | 473874 |
| Unique reflections | 139311 | 67074 |
| Molecules per asymmetric unit | 2 | 2 |

Data Refinement

| | ACDH-11 w/ C11-CoA | ACDH-11 w/o C11-CoA |
|---|---|---|
| Resolution range | 50-1.8 | 50-2.27 |
| $R_{work}$/ $R_{free}$ (%)†† | 14.6 / 18.6 | 16.7 / 22.3 |
| r.m.s.d. Bond lengths (Å) | 0.019 | 0.017 |
| r.m.s.d. Bond angle () | 1.972 | 1.817 |
| Average B-factors (Å$^2$) | | |
| Protein | 53.1 / 51.9 | 42.8 / 48.4 |
| FAD | 65.53 / 53.6 | 46.6 / 36.6 |

| | | |
|---|---|---|
| C11-CoA | N.A. | 52.1 / 53.3 |

Values in parentheses are for the highest resolution shell.

†$R_{merge}$ = $\left| \sum_{hkl} \sum_j \sum \boldsymbol{I}_j - \langle I \rangle \right| / \sum_{hkl} \sum_j \sum \boldsymbol{I}_j$ where $\langle I \rangle$ is the mean intensity of j observations of reflection hkl and its symmetry equivalents.

††$R_{work}$ = $\sum_{hkl} \left| F_{obs} \_ kF_{calc} \right| / \sum_{hkl} \left| F_{obs} \right|$ where k is a scale factor, for 95% of reflections that were used in refinement. $R_{free}$ = $R_{work}$ for 5% of reflections excluded from crystallographic refinement.

## Supplemental References


Adams, P.D., Afonine, P.V., Bunkoczi, G., Chen, V.B., Davis, I.W., Echols, N., Headd, J.J., Hung, L.W., Kapral, G.J., Grosse-Kunstleve, R.W.*, et al.* (2010). PHENIX: a comprehensive Python-based system for macromolecular structure solution. Acta Crystallogr D Biol Crystallogr *66*, 213-221.

Battaile, K.P., Molin-Case, J., Paschke, R., Wang, M., Bennett, D., Vockley, J., and Kim, J.J. (2002). Crystal structure of rat short chain acyl-CoA dehydrogenase complexed with acetoacetyl-CoA: comparison with other acyl-CoA dehydrogenases. J Biol Chem *277*, 12200-12207.

Kim, J.J., Wang, M., and Paschke, R. (1993). Crystal structures of medium-chain acyl-CoA dehydrogenase from pig liver mitochondria with and without substrate. Proc Natl Acad Sci U S A *90*, 7523-7527.

Ma, D.K., Rothe, M., Zheng, S., Bhatla, N., Pender, C.L., Menzel, R., and Horvitz, H.R. (2013). Cytochrome P450 drives a HIF-regulated behavioral response to reoxygenation by *C. elegans*. Science *341*, 554-558.

Ma, D.K., Vozdek, R., Bhatla, N., and Horvitz, H.R. (2012). CYSL-1 interacts with the O2-sensing hydroxylase EGL-9 to promote H2S-modulated hypoxia-induced behavioral plasticity in C. elegans. Neuron *73*, 925-940.

McAndrew, R.P., Wang, Y., Mohsen, A.W., He, M., Vockley, J., and Kim, J.J. (2008). Structural basis for substrate fatty acyl chain specificity: crystal structure of human very-long-chain acyl-CoA dehydrogenase. J Biol Chem *283*, 9435-9443.

Murshudov, G.N., Vagin, A.A., and Dodson, E.J. (1997). Refinement of macromolecular structures by the maximum-likelihood method. Acta Crystallogr D Biol Crystallogr *53*, 240-255.

Ringstad, N., and Horvitz, H.R. (2008). FMRFamide neuropeptides and acetylcholine synergistically inhibit egg-laying by *C. elegans*. Nat Neurosci *11*, 1168-1176.

Rodriguez, M., Snoek, L.B., De Bono, M., and Kammenga, J.E. (2013). Worms under stress: *C. elegans* stress response and its relevance to complex human disease and aging. Trends Genet *29*, 367-374.